

Contents lists available at ScienceDirect

Palaeogeography, Palaeoclimatology, Palaeoecology

journal homepage: www.elsevier.com/locate/palaeo



Marine redox variability from Baltica during extinction events in the latest Ordovician–early Silurian



Seth A. Young^{a,*}, Emily Benayoun^a, Nevin P. Kozik^a, Olle Hints^b, Tõnu Martma^b, Stig M. Bergström^c, Jeremy D. Owens^a

- a Department of Earth, Ocean and Atmospheric Science and National High Magnetic Field Laboratory, Florida State University, Tallahassee, FL 32306, USA
- Department of Geology, Tallinn University of Technology, Ehitajate tee 5, 19086 Tallinn, Estonia
- c School of Earth Sciences. The Ohio State University. Columbus. OH 43210. USA

ARTICLE INFO

Keywords:
Hirnantian
Llandovery
Trace metals
Iron
Anoxia
Sulfur isotopes
Euxinia

ABSTRACT

It is well documented that Upper Ordovician and Silurian successions record multiple marine turnover events including the second-largest mass extinction in the Phanerozoic - widespread glaciation, and multiple global carbon cycle perturbations. Whereas causal mechanisms for the Late Ordovician major mass extinction event involving climate, paleoceanographic variation, and δ^{13} C records have been published, similar records remain poorly constrained for subsequent extinction events in the early Silurian. Here, we present new organic matter carbon isotope ($\delta^{13}C_{org}$) chemostratigraphy and corresponding paleoredox proxies (Fe speciation, [Mn, V, Mo], and pyrite sulfur isotopes) from two organic-rich drill core sections in Sweden and Latvia that span the upper Katian through lower Wenlock stages (446-431 Ma). Pyritized Fe and bulk sedimentary Mn concentrations from Upper Ordovician strata in southern Sweden suggest a local redox shift to more reducing conditions in the late Hirnantian, possibly including euxinic (anoxic and sulfidic water column) conditions that coincide with the second mass extinction pulse. The new high-resolution $\delta^{13}C_{org}$ and $\delta^{34}S_{pyr}$ datasets from the late Aeronian (early Silurian) interval within both drill cores show positive excursions that are broadly coincident with the associated Sandvika and sedgwickii extinction events. Independently, Fe speciation and bulk sedimentary trace metal data from this late Aeronian interval record locally euxinic conditions in both the deep basinal (Sweden) and distal shelf (Latvia) settings before and during the late Aeronian positive δ^{13} C excursion. This multiproxy paleoredox dataset provides the first direct evidence for local to regional expansion of reducing marine conditions coincident with this early Silurian (late Aeronian) biotic event and positive δ^{13} C excursion. Additionally, new δ^{34} S_{pyr} values spanning the Llandovery/Wenlock boundary interval in the Latvia core show a positive excursion coincident with Fe speciation and trace metal enrichments that imply a local redox perturbation with intermittently euxinic bottom waters during the rising limb of the Ireviken positive δ^{13} C excursion. The combination of these geochemical data for local- to regional-scale (more data required for global interpretations) changes in marine redox conditions with paleobiological records and evidence for eustatic sea-level rise indicate that environmental stresses related to an expansion of anoxic to euxinic conditions were a probable driver for several extinction events during the latest Ordovician-early Silurian.

1. Introduction

Environmental changes throughout the Ordovician and Silurian periods were a dominant primary control on the mode and tempo of early Phanerozoic animal evolution and extinction. This interval of the Paleozoic was characterized by a global greenhouse-to-icehouse climatic transition, dramatic fluctuations in sea level, multiple marine extinction events, and numerous positive carbon isotope (δ^{13} C) excursions (Frakes et al., 1992; Jeppsson, 1998; Haq and Schutter, 2008;

Trotter et al., 2008; Saltzman and Thomas, 2012; Ghienne et al., 2014; Crampton et al., 2016; Rasmussen et al., 2016, 2019). The first major mass extinction event of the Phanerozoic, the Late Ordovician mass extinction (LOME; ~444 Ma), resulted in the loss of ~85% of marine animal species and ~ 26% of animal families (Sepkoski, 1981; Brenchley et al., 1994; Harper et al., 2014). The LOME has been associated with the Hirnantian positive carbon isotope excursion (HICE), which has been documented from multiple paleocontinents and basins globally (e.g., Kump et al., 1999; Bergstrom et al., 2016; LaPorte et al.,

E-mail address: sayoung2@fsu.edu (S.A. Young).

^{*} Corresponding author.

2009; Zhang et al., 2009). Numerous possible kill mechanisms have been proposed for the LOME including climatic cooling and habitat loss linked to sea-level decrease, large igneous province emplacement, and widespread anoxia or potentially euxinia in the global oceans (Brenchley et al., 2001; Finnegan et al., 2012; Hammarlund et al., 2012; Jones et al., 2017).

Within the succeeding Llandovery Epoch of the Silurian (~443 to 433 Ma) there are three known extinction events: a Rhuddanian extinction event (Cystograptus vesiculosus to Coronograptus cyphus graptolite zones), a late Aeronian extinction event (Lituigraptus convolutus to Stimulograptus sedgwickii graptolite zones), and an early Telychian extinction event (Spirograptus turriculatus to Streptograptus crispus graptolite zones) (e.g., Melchin et al., 1998). Additionally, there is a wellknown and globally documented extinction event that spans the Llandovery-Wenlock boundary (Cyrtograptus murchisoni to early Monograptus riccartonensis zones) (e.g., Loydell, 2007; Cramer et al., 2010). The Rhuddanian bioevent is largely documented in graptolite paleontological data where extinction and origination rates increased in concert yielding only minor global impacts to this clade (Cooper et al., 2014). Late Aeronian paleontological records document an extinction event among several marine groups known as the 'Sandvika Event' (e.g, Aldridge et al., 1993; Jeppsson, 1998), and Stimulograptus sedgwickii Event in graptolites (Melchin et al., 1998). An early Telychian extinction interval was first recognized in graptolites, known as the Utilis Event (Loydell, 1994; Storch, 1995), and it partially overlaps with an extinction in conodonts known as the 'Valgu Event' (Munnecke and Mannik, 2009). Positive carbon isotope excursions (CIEs) are coincident with the late Aeronian, early Telychian, and Llandovery-Wenlock boundary biotic events (Kaljo and Martma, 2000; Kaljo et al., 2003; Cramer and Saltzman, 2005, 2007; Melchin and Holmden, 2006; Fryda and Storch, 2014; Bancroft et al., 2015; Waid and Cramer, 2017; McAdams et al., 2017).

Extreme oxygen deficiency has been linked to several major marine extinction events during the early Paleozoic via geochemical proxy records for widespread anoxic and/or euxinic (sulfidic) water column conditions (Gill et al., 2011a, 2011b; Edwards et al., 2018; Bowman et al., 2019). There is increasing consensus using independent geochemical proxies from multiple ocean basins that marine redox conditions varied and played a mechanistic role in the LOME (Zou et al., 2018). However, proxy records constraining the paleoredox conditions for the recovery interval of this extinction in the early Silurian (Rhuddanian Stage) are undocumented even though there was widespread organic-rich black shale deposition during this time (Melchin et al., 2013). Carbon isotope chemostratigraphic studies, combined with the sedimentological and paleontological work, provide the framework for previously proposed Silurian ocean-climate models (e.g., Bickert et al., 1997; Jeppsson, 1998; Cramer and Saltzman, 2007). However, the links between extinction, marine redox state, global weathering rates, and atmospheric pO2 and pCO2 levels are not well constrained, and thus the mechanisms driving these Llandovery events are largely unconstrained. A combined multiproxy geochemical approach allows for the direct testing of stratigraphic extent and magnitude of local to regional redox perturbations associated with these known CIEs and extinction events. In this study, we have investigated two organic-rich shale to marl successions from Baltoscandia that span the Upper Ordovician-Lower Silurian (upper Katian-lower Sheinwoodian stages), one drill core from Scania, southern Sweden and another from western Latvia (Fig. 1) with previous detailed biostratigraphic studies (Koren et al., 2003; Loydell et al., 2003; Maletz et al., 2014). We present new organic matter carbon isotope ($\delta^{13}C_{org}$) and sedimentary pyrite sulfur isotope ($\delta^{34}S_{pyr}$) measurements, iron speciation, and trace metal concentrations (molybdenum, vanadium, manganese). Our Late Ordovician geochemical datasets provide independent local constraints on previous marine redox proxies that have been proposed for the LOME. Furthermore, our integrated multiproxy geochemical datasets are some of the first to constrain local to regional marine redox conditions to discern the possible mechanism(s) responsible for the known extinction records from the early Silurian.

2. Background

2.1. Geologic setting

The paleocontinent of Baltica was approaching equatorial latitudes during the Late Ordovician-early Silurian (Fig. 1), and the closure of the Tornquist Sea continued throughout the collisional tectonic events that began to dock Avalonia along the southwestern margin of Baltica (Vecoli and Samuelsson, 2001; Lees et al., 2002; Cocks and Torsvik, 2002). The nearby Iapetus Ocean was also narrowing, although final closure did not occur until the late Silurian-Early Devonian during the Caledonian Orogeny (van Staal et al., 2009). The Röstånga-1 core was drilled in the province of Scania, Sweden and is located within the structurally complex Tornquist Zone that separates the Baltica from the rest of the European continent (Bergström et al., 1999; Bergstrom et al., 2016). The Röstånga-1 core contains predominantly organic-rich shales and mudstones deposited within a foreland basin along the southern margin of Baltica during the Late Ordovician through early Silurian (Katian through Telychian stages). The Röstånga-1 core is presumed to have been deposited within the deeper parts of a foreland basin (~1000 ± 300 m; Bjerreskov and Jørgensen, 1983). Previous biostratigraphic work constrains the light to medium grey mudstones with rare marl/limestone beds of the upper Lindegård Formation to the Metabolograptus persculptus and Avitograptus avitus graptolite biozones of the late Hirnantian Stage (Bergström et al., 1999; Koren et al., 2003). The overlying finely laminated (mm-scale) black shales and medium grey mudstones/shales of the Kallholn Formation lies within the Akidograptus ascensus through S. crispus graptolite biozones of Rhuddanian through Telychian stages (Bergström et al., 1999; Koren et al., 2003), A considerable biostratigraphic gap is present at 35.4 m level within the Röstånga-1 core; this apparent hiatus spanned the early Aeronian Demirastrites triangulatus through part of the Pribylograptus leptotheca graptolite biozones (Maletz et al., 2014).

The strata preserved within the Aizpute-41 core from western Latvia (Fig. 1B) were deposited in a distal-shelf environment on the eastern side of the Baltic Basin during the early Silurian (Kiipli, 2004; Kiipli et al., 2009). Additionally, strata from this core locality were most likely deposited below storm wave base as there are no obvious sedimentary structures found to indicate local storm or wave action (Kiipli et al., 2004, 2009). Previous biostratigraphic work constrains the interbedded shales and thin argillaceous limestones of the Remte Formation to the Rhuddanian Stage within the C. cyphus graptolite biozone and Distomodus kentuckyensis conodont biozone (Loydell et al., 2003). The overlying finely laminated black shales of the Dobele Formation are latest Rhuddanian through Aeronian in age, constrained to the upper C. cyphus through S. sedgwickii graptolite biozones and Pseudolonchodina expansa through D. staurognathoides conodont biozones (Loydell et al., 2003). The overlying Jurmala Formation consists largely of laminated green to red marlstones with minor intervals of bioturbation deposited during the Telychian, S. turriculatus through C. lapworthi graptolite biozones and D. staurognathoides through Pterospathodus amorphognathoides conodont biozones (Loydell et al., 2003). The laminated green to brown marlstones of the Riga Formation are early Wenlock in age (Sheinwoodian Stage) constrained by C. murchsoni through M. riccartonensis graptolite biozones and P. amorphognathoides through Kockelella ranuliformis conodont biozones (Loydell et al., 2003; Cramer et al., 2010). Additionally, numerous K-bentonites identified in the Aeronian-Telychian strata of the Aizpute-41 drill core provide radiometric dating constraints and correlations across Baltica (Kiipli et al., 2013, 2014).

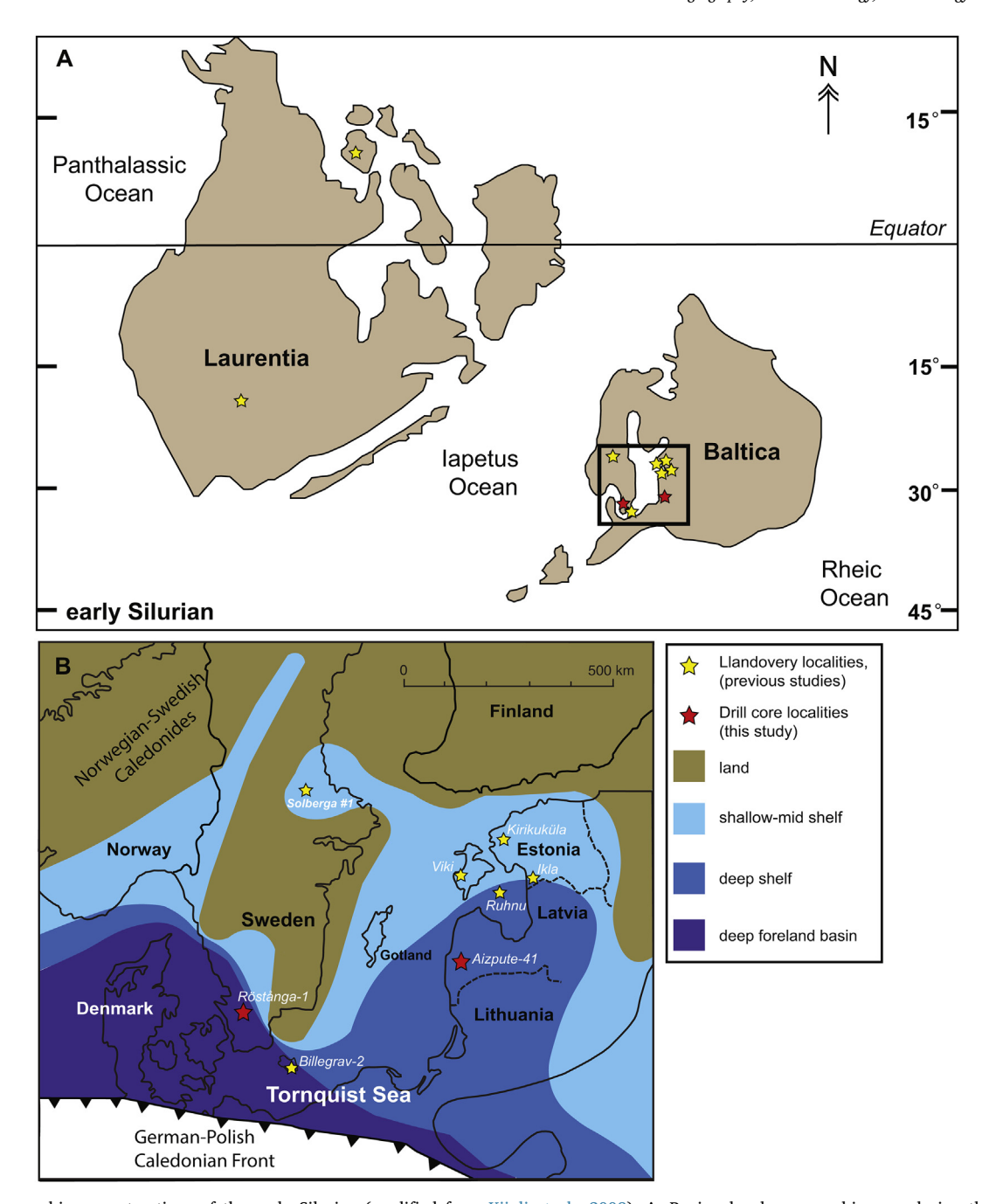


Fig. 1. Paleogeographic reconstructions of the early Silurian (modified from Kiipli et al., 2009). A, Regional paleogeographic map during the early Silurian (~440 Ma), showing locations of the early Silurian study areas (previous studies include Kaljo and Martma, 2000; Melchin and Holmden, 2006; Cramer et al., 2010; Hammarlund et al., 2012; Bancroft et al., 2015; McAdams et al., 2017; Waid and Cramer, 2017). B, Inset map showing locations of the Aizpute-41 and Röstånga-1 drill cores in the Baltic Basin and distribution of facies belts (modified from Loydell et al., 2003; Bergstrom et al., 2016).

2.2. Carbon and sulfur isotopes

Variations in the carbon isotope compositions of marine carbonates ($\delta^{13}C_{carb}$) are used to interpret perturbations in the global carbon cycle throughout geologic history, specifically as a proxy for intervals of enhanced burial of isotopically light organic carbon and at times an important tool for stratigraphic correlation (e.g., Saltzman and Thomas, 2012). Carbon isotopes of organic-rich marine sediments ($\delta^{13}C_{org}$) have been utilized to represent local changes in carbon cycling as sedimentary total organic carbon (TOC) can be affected by photosynthetic fractionation associated with carbon fixation by marine primary producers, organic matter source variations, secondary biological fractionation (i.e. heterotrophy), and diagenesis (Hayes et al., 1999; Kienast

et al., 2001; Royer et al., 2001). Additionally, $\delta^{13}C_{org}$ values can also be used to interpret changes in the global DIC reservoir if $\delta^{13}C_{org}$ values are shown to covary with correlative $\delta^{13}C_{carb}$ values and local organic matter source and secondary effects have not significantly impacted the observed trends in $\delta^{13}C_{org}$ data (e.g., Patzkowsky et al., 1997; Joachimski et al., 2002; LaPorte et al., 2009).

Sulfur plays a critical role in regulating the partial pressure of atmospheric oxygen (pO_2) on geologic time scales and is dynamically cycled between inorganic reservoirs and organic substrates through a series of oxidation/reduction reactions via abiotic and biotic processes (e.g., Berner, 1985; Fike et al., 2015). Microbial sulfate reduction (MSR) couples the long-term carbon and sulfur cycles via anerobic respiration of marine organic matter, and oceanic sulfate levels are linked to

atmospheric O_2 content via oxidative weathering of pyrite and other terrestrial sulfide minerals (e.g., Berner, 2006 and references therein). Sedimentary pyrite (FeS₂) and its precursor minerals are quickly formed through reactions with hydrogen sulfide (H₂S), which is a by-product of microbial sulfate reducers metabolism, and dissolved Fe²⁺ (Canfield et al., 1992). MSR in modern marine environments predominantly occurs within the sediments, however, when this process takes place in the water column it has dramatic consequences on life due to the toxicity of H₂S to most aerobic organisms (Vaquer-Sunyer and Duarte, 2010).

Parallel trends in δ^{13} C and δ^{34} S records from multiple stratigraphic sections have been used to interpret and quantify global oceanic redox conditions (e.g, Gill et al., 2011a, 2011b; Owens et al., 2013; Young et al., 2019). Expansion of reducing conditions globally can lead to the increased burial rates of organic carbon and pyrite, which subsequently lead to parallel positive seawater trends in δ^{13} C and δ^{34} S_{CAS} (carbonate-associated sulfate) values recorded in marine carbonate sequences. Additionally, sedimentary pyrite contents and δ^{34} S_{pyr} records have the potential to constrain local redox conditions as δ^{34} S_{pyr} values are sensitive to the location of pyrite formation (e.g., within the reducing water column, sediment-water interface, and/or within sediments) and availability of reactive iron (Lyons, 1997; Gomes and Hurtgen, 2015).

2.3. Iron geochemistry

Iron geochemistry from organic-rich shales and mudstones are used to constrain local redox conditions using the ratios of various groups of Fe minerals. The total iron to aluminum ratio (Fe_T/Al) can be used as a paleoredox proxy to interpret anoxic deposition (Lyons and Severmann, 2006), ratio enrichments greater than Phanerozoic averages for oxic marine mudstones/shales suggest reducing conditions (0.53 ± 0.1; Raiswell et al., 2008). The ratio of highly reactive iron (FeHR) to total iron (Fe_T) can also indicate an anoxic depositional setting due to the relatively large fraction of reactive iron that is common in these environments (Poulton and Canfield, 2011). Marine mudstones contain highly reactive iron minerals, such as pyrite, magnetite, siderite, and ankerite, which together define the highly reactive iron pool, FeHR (e.g., Poulton et al., 2004; Poulton and Canfield, 2005, 2011). These ironbearing mineral phases (FeHR) are enriched relative to FeT in sediments deposited beneath anoxic waters that are ferruginous (anoxic and Fe²⁺rich, sulfate-limited) or euxinic (anoxic and sulfide-rich, iron-limited) (e.g., Raiswell et al., 2018). Thus, FeHR/FeT values above the threshold of 0.38 indicated deposition under an anoxic water column with enhanced Fe delivery, however values between 0.22 and 0.38 may represent an anoxic water column with high sedimentation rates or other variables that may mask any Fe enrichments (Poulton and Canfield, 2011; Raiswell et al., 2018). In sulfidic water columns (euxinic) or sulfidic pore fluids, most of the iron for pyrite formation (Fe_{DV}) is from iron oxyhydroxides and carbonate minerals that are reactive to hydrogen sulfide on short, early diagenetic time scales (< 104 yr; e.g., Canfield et al., 1992; Raiswell and Canfield, 1996). The ratio of pyrite iron (Fe_{pv}) to Fe_{HR} is used to track the degree that the Fe_{HR} pool is converted to pyrite, and an accepted threshold value of 0.70 or larger separates ferruginous from euxinic conditions (März et al., 2008). It is important to note that high Fe_{py}/Fe_{HR} values can be achieved in two contrasting settings, in a euxinic water column or in oxic water column where porewater sulfide accumulates within the sediments at depth (Hardisty et al., 2018).

2.4. Trace metal geochemistry

The cycling of bio-essential and redox-sensitive trace metals such as molybdenum (Mo) and many others can be used to track changes in primary productivity and redox states of the ocean (e.g., Algeo and Maynard, 2004; Scott et al., 2008; Gill et al., 2011a, 2011b; Owens et al., 2012, 2016, 2017; Reinhard et al., 2013). Furthermore, with

independent constraints on local redox from iron geochemistry interpretations of trace metal enrichments can be used to infer global redox shifts from oxic to anoxic conditions (V, Cr, Zn), and euxinic conditions (Mo). Molybdenum, primarily in the form of molybdate (MoO_4^{2-}) , is the most abundant transition metal in the modern well-oxygenated oceans (e.g., Tribovillard et al., 2006) and has a relatively long residence time of ~450 kyr (e.g., Miller et al., 2011). The primary input of Mo to the oceans is oxidative weathering of sulfide minerals (i.e., pyrite) via rivers (e.g., Miller et al., 2011). Under oxic conditions, Mo is readily adsorbed by Mn- and Fe-oxides when the chemocline is below the sediment-water interface (e.g., Algeo and Tribovillard, 2009). However. Mo is most efficiently buried in the presence of free sulfide. either in the water column or within the sediment porewaters, with the former considerably more efficient (Scott and Lyons, 2012). Significant Mo enrichments (20 to > 100 ppm) in the geologic record can be interpreted as deposition under euxinic water column conditions or sulfidic pore waters under an anoxic water column (e.g., Hardisty et al., 2018). Vanadium (V) in the modern ocean is characterized by a smaller reservoir size and shorter residence time (~50 to 100 kyr) relative to Mo (Algeo, 2004). Marine [V] are primarily controlled by the burial flux as vanadate oxyanions (HVO₄²⁻ and HVO₄⁻) associated with Mnand Fe-oxides and efficiently buried under low oxygen conditions (e.g., Tribovillard et al., 2006). Vanadium is actively incorporated into marine sediments in low oxygen conditions and continues to be sequestered under euxinic conditions (Algeo, 2004). Therefore, enrichment of V in marine sediments can occur independently of free sulfide, unlike Mo which requires sulfidic conditions for reductive enrichment. Thus, trends in [V] can be used as an indicator of low oxygen to anoxic conditions which has been suggested for global differential trace metal drawdown (Owens et al., 2016).

Manganese (Mn) concentrations can also be used as local redox proxy due to its rapid response to changes in local oxygen conditions. Oxidized Mn (III/IV) is rapidly reduced to Mn²⁺, due to its high redox potential, as oxygen concentrations decrease in dysoxic to anoxic conditions (Rue et al., 1997; Algeo and Maynard, 2008). As a result, Mnoxides under low oxygen conditions are dissolved, soluble Mn²⁺ is recycled into the water column, allowing for the possible deposition of other types of Mn-minerals (e.g., sulfides, carbonates; Force and Cannon, 1988; Force and Maynard, 1990; Dickens and Owen, 1994; Algeo and Maynard, 2004; Owens et al., 2017). Thus total sedimentary Mn concentrations enriched above-average crustal values of 850 ppm (Turgeon and Brumsack, 2006; Boyer et al., 2011) likely represent more oxidizing conditions.

3. Methods

3.1. Samples

The Aizpute-41 core is housed at the Tallinn University of Technology in Estonia where it was sampled and described (additional information at https://geocollections.info/locality/156). Lithologic samples were collected at 10 cm to 1-m intervals from the Aizpute-41 core for geochemical analyses at Florida State University (FSU). The Röstånga-1 core is archived at Lund University in Sweden where it was described and sampled, and lithologic samples were collected at halfmeter intervals for geochemical analyses at FSU. Samples were selected from horizons of the cores that have no obvious signs of recrystallization, secondary calcite veins, K-bentonite beds, and pyrite nodules were avoided. Samples were sonicated in ultrapure (deionized, 18.2 $\mathrm{M}\Omega$) water to remove any potentially weathered surfaces and drilling mud residues, dried, and subsequently powdered using an agate mortar and pestle.

3.2. Organic carbon isotopes

In total 170 samples were analyzed for $\delta^{13}C_{\rm org}$ from the Aizpute-41

and Röstånga-1 cores. Approximately ~0.5 g of powdered shale samples were weighed and then reacted with 6 N HCl. Each sample was acidified and centrifuged three times to remove all carbonate minerals. The remaining insoluble residues were then rinsed in ultrapure (deionized, 18.2 M Ω) water three times to remove all HCl, and then the samples were placed in a 70 °C oven to dry overnight. The residues were then homogenized and weighed into tin capsules for isotopic analysis. The carbon isotopic ratios of the samples were then measured using a Carlo Erba Elemental Analyzer coupled to the ThermoFinnegan Delta Plus XP isotope ratio mass spectrometer (IRMS) via a Conflo-III device at the National High Magnetic Field Laboratory at FSU (NHMFL-FSU). Sample precision and calibration of data are done through routine analyses of laboratory standards that are calibrated against IAEA standards. Standards include: Acetanilide (-29.2%), Urea 2 (-8.13%) and WYSTD (-12.7%), with standard deviations for $\delta^{13}C_{org}$ of \pm 0.2% and \pm 0.7% for %C (1 σ) or better. All carbon isotope results are reported in standard delta-notation (δ) with units reported as per mil (%) relative to the VPDB (Vienna Pee Dee Belemnite) standard for δ^{13} C. The weight percent of total organic carbon (TOC) in the samples was determined by comparison of voltages for the ion beam intensities of masses 44, 45, and 46 ${\rm CO_2}^+$ between our samples and known wt% carbon of the gravimetric standard Acetanilide. The uncertainty of these TOC measurements is better than \pm 5%.

3.3. Pyrite sulfur isotopes

Sedimentary pyrite was extracted from 116 samples, taken from both the Aizpute-41 and Röstånga-1 cores, using the standard chromium reducible sulfur extraction but modified following Bruchert and Pratt (1996). Approximately 0.5-2.0 g of powdered samples were weighed into an extraction flask. Pyrite sulfur was extracted from the samples using a mixture of \sim 70 ml of 12 M HCl and \sim 30 ml of 1.0 M chromium chloride (CrCl2·6H2O) that was heated and continuously stirred in an N2-purged extraction flask. Evolved H2S gas was passed through a buffered solution (0.1 M sodium citrate) and then into a 0.1 M AgNO_3 solution to precipitate Ag₂S for ~2–3 h. Subsequently, the Ag₂S precipitate was then filtered, rinsed, dried, and weighed for concentration determinations. Ag₂S powders were then weighed into tin cups along with 2-5 mg of V₂O₅ for sulfur isotope analysis using a Thermo Isolink Elemental Analyzer coupled to a Thermo Delta V Plus IRMS via a Conflo-IV open split interface at the NHMFL-FSU. All sulfur isotope results are reported in standard delta-notation (δ) with units reported in per mil (%) relative to VCDT (Vienna-Cañon Diablo Troilite). Samples are calibrated to internal laboratory standards EMR-CP (+0.9%), PQM2 (-16.0%), ERE (-4.7%), PQB-D (+40.5%), and SWP (+20.3‰) with standard deviations of \pm 0.2‰ (1 σ) or better. In addition to sulfur isotope analysis, the total amount of Ag₂S precipitate was gravimetrically determined to calculate weight percent pyrite, assuming quantitative stoichiometry of FeS2 to Ag2S which was used to calculate pyrite Fe (Fepy).

3.4. Iron speciation

Ninety-seven samples were selected to be analyzed for sequential Fe extractions (Fe speciation) from the Aizpute-41 and Röstånga-1 cores following methods outlined by Poulton and Canfield (2005). Approximately 0.1 g of powdered rock samples were weighed into 15 ml centrifuge tubes. First, Fe from carbonate minerals (Fe $_{\rm carb}$) was extracted using 10 ml of 1.0 M sodium acetate solution buffered to pH 4.5 with 48 h of continuous shaking. Second, Fe from oxides and oxyhydroxide minerals (Fe $_{\rm ox}$) was extracted using 10 ml of 0.29 M sodium dithionite buffered to pH 4.8 with 0.35 M acetic acid and 0.2 M sodium citrate for 2 h with constant shaking. Third, Fe in the phase of magnetite (Fe $_{\rm mag}$) was extracted from the remaining residue using 0.2 M ammonium oxalate and 0.17 M oxalic acid buffered with ammonium hydroxide to pH 3.2 for 6 h with continuous shaking. Following each of the three

sequential Fe extractions, samples were centrifuged and supernate saved for geochemical analysis. Subsequently, centrifuged samples were rinsed and agitated with ultrapure water, centrifuged again, and decanted before progressing to the next sequential extraction step. Supernate of each extraction was diluted using 2% ultrapure HNO $_3$, and analyzed for Fe concentrations using an Agilent 7500cs inductively-coupled plasma mass spectrometer (ICP-MS) at the NHMFL-FSU. Highly reactive Fe (Fe $_{HR}$) is calculated as the sum of these species: Fe $_{carb}$ + Fe $_{ox}$ + Fe $_{mag}$ + Fe $_{py}$. Duplicate samples had a reproducibility of 7% for the entire extraction method which is similar to other labs.

3.5. Elemental concentrations

Bulk elemental composition of the same 97 samples analyzed for sequential iron speciation (described above) was determined through multi-acid digestion. Sample masses of 50-100 mg were weighed into Teflon beakers and microwave digested using a CEM MARS 6 instrument to remove organic carbon without volatilizing redox-sensitive trace elements. Samples were completely dissolved using a standard multi-step trace metal acid digestion using various combinations of trace-metal free HNO3, HCl, and HF. These acids were added to the samples with heat (~120-180 °C) for 24-48 h, and dried down before having adding additional more acid. If organic matter was present in sample solutions post-microwave digestion, it was then oxidized using ultrapure H₂O₂. After complete dissolution of the samples, they were dried down and dissolved in 2% HNO3 for analysis on an Agilent 7500cs quadrupole ICP-MS for trace metal concentrations at the NHMFL-FSU. International reference material (USGS standards SDO-1, SCO-1, and SGR-1), were dissolved simultaneously and were all within the accepted analytical ranges for all reported elements. All results are reported in parts per million (ppm) with an analytical precision of \pm 5% or better for Mo, V, and Mn. Procedural blanks were below detection limits.

4. Results

4.1. Röstånga-1 core, Sweden

Carbon isotopes within the upper part of the Lindegård Formation (68 m to 65 m) have initial baseline $\delta^{13}C_{org}$ values that range between -30.0% and -29.5%, and $\delta^{13}C_{org}$ values are perturbed abruptly to $\sim -26.5\%$ at 64 m interval within the drill core (Fig. 2). The $\delta^{13}C_{org}$ values remain isotopically more positive for ~20 m (up to the 54 m interval) where they begin to return to a new baseline of $\sim -31.5\%$ within the upper M. persculptus and A. avitus graptolite biozones of the Hirnantian Stage. The $\delta^{13}C_{org}$ values remain stable between -31.5%and - 29.5% within the upper A. avitus through C. vesiculosus graptolite biozones. At 34 m, within the late Aeronian L. convolutus graptolite biozone, $\delta^{13}C_{org}$ values begin to shift positively from these previous baseline values and reach a maximum value of -27.4% in the S. sedgwickii graptolite biozone. In the S. guerichi graptolite biozone $\delta^{13}C_{org}$ values return to a new baseline of -29.0%. At 13 m within the core $\delta^{\tilde{1}3}C_{\mathrm{org}}$ values shift positively from baseline values of -29.5% to a maximum recorded value of -27.7% at the top of the core within the Streprograptus crispus graptolite biozone.

The $\delta^{34}S_{py}$ values within the Lindegård and Kallholn formations document a broadly coupled trend with $\delta^{13}C_{org}$ values (Fig. 2). In the upper Katian–Hirnantian topmost Lindegård Formation $\delta^{34}S_{py}$ values shift positively from a baseline average of $\sim -8\%$ to $\sim +4\%$, coinciding with higher $\delta^{13}C_{org}$ values, and then $\delta^{34}S_{py}$ values fall back to $\sim -25\%$ in the upper *M. persculptus* and *A. avitus* graptolite biozones. The $\delta^{34}S_{py}$ values shift positively in the late Aeronian *L. convolutus* graptolite biozone from baseline values of -29% to -6.5% within the *S. sedgwickii* graptolite biozone that corresponds to peak $\delta^{13}C_{org}$ values within the same interval of the drill core. In the grey shale/mudstone facies (*S. crispus* graptolite biozone) near the top of the core, $\delta^{34}S_{py}$ values shift positively from a baseline of -32% to a maximum of

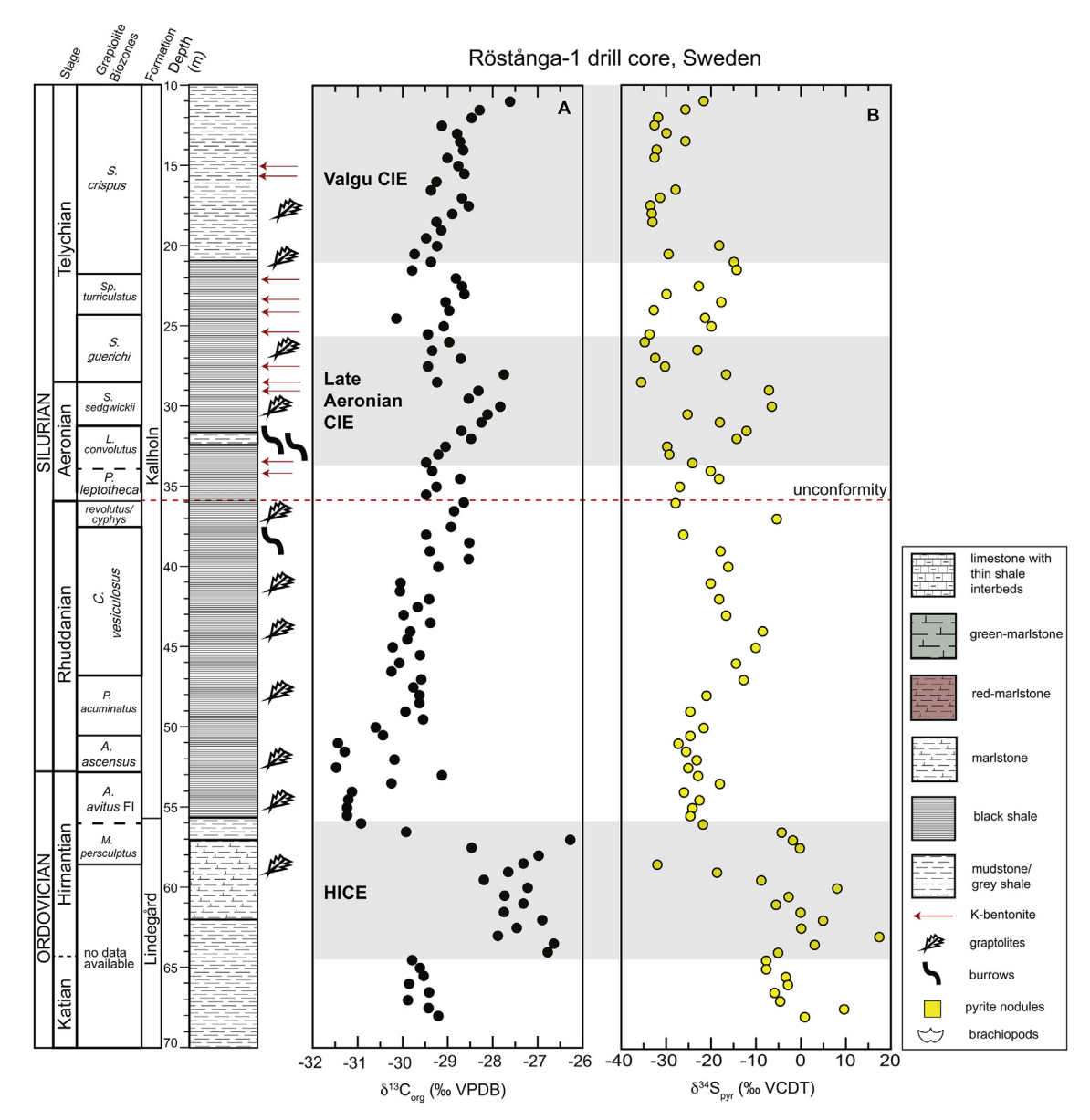


Fig. 2. Late Ordovician–early Silurian stable isotopic data ($\delta^{13}C_{org}$ and $\delta^{34}S_{py}$) from the Röstånga-1 drill core, Sweden. Graptolite biozones are plotted from previous biostratigraphic studies (Bergström et al., 1999; Koren et al., 2003; Maletz et al., 2014). Grey bars denote globally documented positive carbon isotope excursions (CIEs), including the HICE–Hirnantian carbon isotope excursion.

-22% that corresponds to the rising $\delta^{13}C_{\rm org}$ values from the same interval

Iron geochemistry was analyzed on a series of samples throughout the Lindegård and Kallholn formations (Fig. 3A-C). The mudstones within the Lindegård Formation (upper Katian-Hirnantian) have an average Fe_T/Al value of 0.62 (the Phanerozoic average), with a range from 0.45 to 0.81. The upper Hirnantian to upper Aeronian (*A. avitus-P. leptotheca* graptolite biozones) black shales of the Kallholn Formation have an average Fe_T/Al value of 0.46, with a range from 0.40 to 0.58. The Fe_T/Al value increase in the upper Kallholn Formation with an average of 0.60, ranging from 0.42 to 0.90.

The ratio of Fe_{HR} to Fe_{T} within the Lindegård Formation trends from values < 0.1 to values of 0.36 within the *M. persculptus* and *A. avitus* graptolite biozones. The Fe_{HR}/Fe_{T} values within the lower Kallholn Formation fluctuates between 0.21 and 0.61, *A. avitus* through *C. cyphus* graptolite biozones, with most samples near the value of 0.22. Fe_{HR}/Fe_{T} values plot above 0.22 in the *P. leptotheca* through lower *S. sedgwickii* graptolite zones except for two data points that fall below this value,

which corresponds to the interval of bioturbated grey mudstone (971.5–972.5 m). Fe $_{\rm HR}/{\rm Fe}_{\rm T}$ values remain below 0.22 for the remainder of the Kallholn Formation (Telychian; *S. guerichi–S. crispus* graptolite biozones) except four data points. Fe $_{\rm py}/{\rm Fe}_{\rm HR}$ values show large variability throughout the Kallholn Formation. The ratio of Fe $_{\rm py}$ to Fe $_{\rm HR}$ within the Lindegård Formation trends stratigraphically from values < 0.1 to values > 0.7 in the upper part of the formation. The Fe $_{\rm py}/{\rm Fe}_{\rm HR}$ ratios in the overlying Kallholn Formation, *A. avitus* through *C. cyphus* graptolite biozones, are mostly > 0.70. In the late Aeronian portion of the Kallholn Formation, *P. leptotheca* through lower *S. sedgwickii* graptolite zones, Fe $_{\rm py}/{\rm Fe}_{\rm HR}$ values are > 0.70 corresponding to the same interval with Fe $_{\rm HR}/{\rm Fe}_{\rm T}$ values > 0.22, except for two data points. The remainder of the upper Kallholn Formation, upper *S. sedgwickii* through *S. crispus* graptolite biozones, records Fe $_{\rm py}/{\rm Fe}_{\rm HR}$ ratios largely (75% of samples) below 0.70.

Trace metal analysis was completed on all samples from the Röstånga-1 core (Fig. 3D-F) that have corresponding iron geochemistry described above. Molybdenum concentrations in the Lindegård

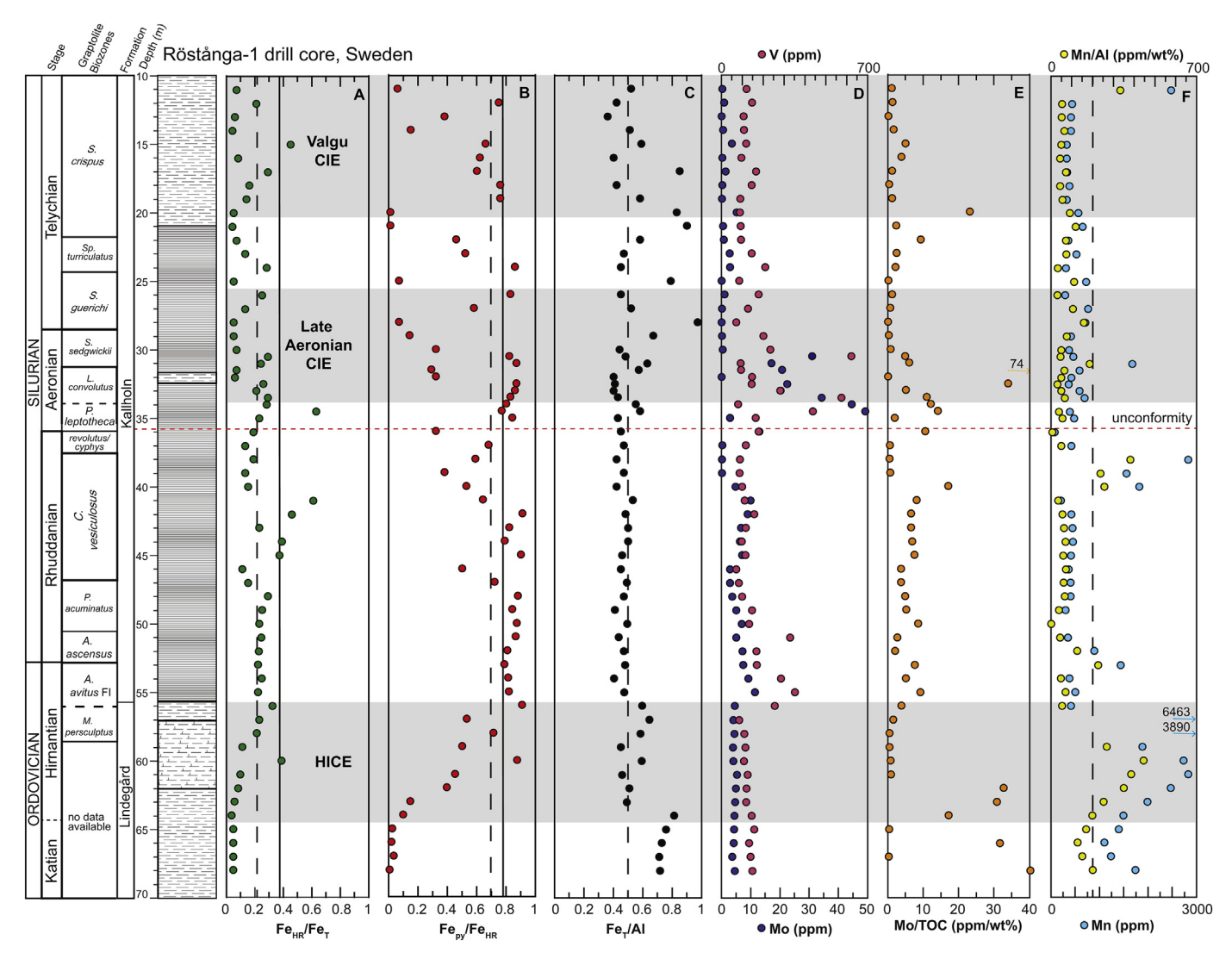


Fig. 3. Late Ordovician–early Silurian paleoredox geochemical data from organic-rich marls and mudstones of the Röstånga-1 drill core, Sweden. Grey bars denote globally documented positive carbon isotope excursions (CIEs), including the HICE–Hirnantian carbon isotope excursion. A, Dashed vertical line and solid line for Fe_{HR}/Fe_T represent the threshold for possibly anoxic (0.22) and anoxic (0.38) bottom waters, respectively. B, Dashed vertical line and solid line for Fe_{py}/Fe_{HR} represent the threshold for possibly euxinic (0.70) and anoxic (0.78) bottom waters, respectively. C and F, dashed vertical line represents Phanerozoic average crustal values for Fe_T/Al and Mn.

Formation average 4 ppm, with a range from 3 to 5 ppm. Mo contents for the overlying black and grey shales of the entire Kallholn Formation are higher than the Lindegård Formation, with an average of 8 ppm, but have a wide range from 1 to 49 ppm. Mo contents are highest in the interval from 35 m to 30 m (P. leptotheca through S. sedgwickii graptolite zones), where concentrations are elevated between 20 and 49 ppm. Vanadium concentrations trend similarly to [Mo] throughout the Lindegård and Kallholn formations, with the majority of the drill core having values below 200 ppm. However, the highest V enrichments (ranging from 437 to 621 ppm) fall within the same interval corresponding to the highest [Mo] in the late Aeronian. Manganese concentrations and Mn/Al ratios show approximately correlative trends throughout the Röstånga-1 drill core (Fig. 3F; Fig. DR 1F). Mn contents from the Lindegård Formation average 2276 ppm (ranging from 406 to 6463 ppm). Mn concentrations in the overlying Kallholn Formation are markedly lower, an average of 618 ppm (Fig. 3F).

4.2. Aizpute-41 core, Latvia

The $\delta^{13}C_{\rm org}$ data recorded from the Aizpute-41 core display a wide range of values from near -30% to -26% (Fig. 4). In the Remte

Formation, $\delta^{13}C_{org}$ values initially range between -27.5%and - 27.0%, and then within the lower C. cyphus Biozone, a shift to more negative baseline values (-29.5% to -29.0%) corresponds to a lithofacies transition from an argillaceous lime mudstone to thinly interbedded limestone and shales. The overlying black shales of the Dobele Formation (upper C. cyphus through L. convolutus graptolite biozones) have $\delta^{13}C_{org}$ values that average - 29.0%, with a range from -29.6% to -28.5%. Within the uppermost 1.5 m of the Dobele Formation (upper L. convolutus through S. sedgwickii graptolite biozones) $\delta^{13}C_{\rm org}$ values shift positively from -29.5% to a maximum value of -27.0%, and then shift back to -28.5% near the contact of Dobele and Jurmala formations. The $\delta^{13}C_{org}$ values in the overlying Jurmala Formation are perturbed positively from -28.5% to -26.5%between 969 and 960 m, and then return to a new baseline of -28.0%in the 950 to 940 m interval (S. turriculatus through Oktavites spiralis graptolite biozones). Within the upper Jurmala-lower Riga formations (Streptograptus lapworthi to C. murchisoni graptolite biozones) $\delta^{13}C_{org}$ values shift positively from -29.0% to -27.0% at the top of the sampled interval within the core (M. firmus- M. riccartonensis graptolite biozones).

The $\delta^{34}S_{py}$ values display largely coupled trends with carbon

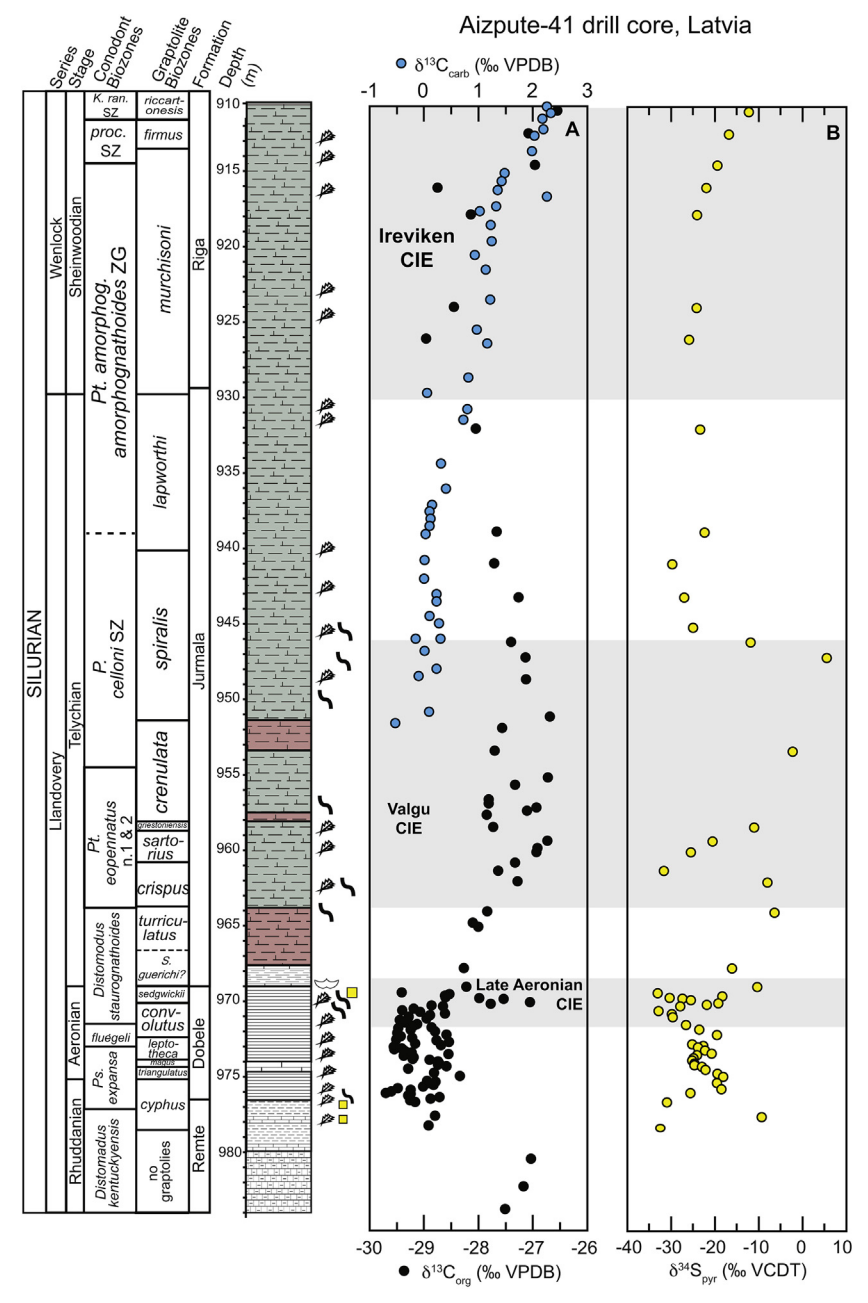


Fig. 4. Llandovery—early Wenlock (early Silurian) stable isotopic data ($\delta^{13}C_{org}$ and $\delta^{24}S_{py}$) from the Aizpute-41 drill core, Latvia. Graptolite and conodont biozones are plotted from previous biostratigraphic studies (Loydell et al., 2003; Cramer et al., 2010). The $\delta^{13}C_{carb}$ data (blue circles) are replotted from Cramer et al. (2010). Please refer to legend in Fig. 2 for lithology and fossil symbols used. Grey bars denote globally documented positive carbon isotope excursions (CIEs). (For interpretation of the references to colour in this figure legend, the reader is referred to the web version of this article.)

isotopes and record a large variation over the extent of the Aizpute-41 core ranging from -30% to +5% (Fig. 4B). In the Remte Formation, $\delta^{34}S_{py}$ values are at -30% in the lower C. cyphus Biozone except for one data point that plots near -10%. Values increase to -20% within the lower Dobele Formation (top of C. cyphus Biozone) and quickly return to -30% near the L. convolutus/S. sedgwickii graptolite biozone boundary. In the S. sedgwickii Biozone $\delta^{34}S_{py}$ values shifts from -33% to a maximum value of -18.4% and then values trend back to -33%, coincident with a positive shift in $\delta^{13}C_{org}$ values. Following this +14% magnitude positive excursion, $\delta^{34}S_{py}$ values are highly variable ranging between -31.7% and +5.4% within the lower to middle Jurmala Formation. In the upper Jurmala Formation (S. lapworthi to C. murchisoni graptolite biozones) $\delta^{34}S_{py}$ values are stable with an average of -25%, and then shift positively in the overlying Riga Formation with a

maximum value of -12%.

Iron geochemistry was also analyzed on samples throughout the core (Fig. 5), with Fe $_T$ /Al values falling below the average crustal values (0.62) for the majority of the section but plot above these values in the upper *S. sedgwickii* through lower *Monoclimacis crenulata* graptolite biozones. The Fe $_{HR}$ /Fe $_T$ values for the Remte Formation are at or slightly above 0.38, and then following the lithofacies transition values fall well below this value. Near the transition to the black shales of the Dobele Formation, Fe $_{HR}$ /Fe $_T$ values shift to values that fall between 0.22 and 0.38. Fe $_{HR}$ /Fe $_T$ values remain above 0.22 (the possibly anoxic threshold) until the very top of the Dobele Formation (upper *S. sedgwickii* graptolite biozone) where values fall below 0.22 and remain low throughout the overlying Jurmala Formation. The Fe $_{py}$ /Fe $_{HR}$ values from the Remte Formation are below 0.70, and then near the transition

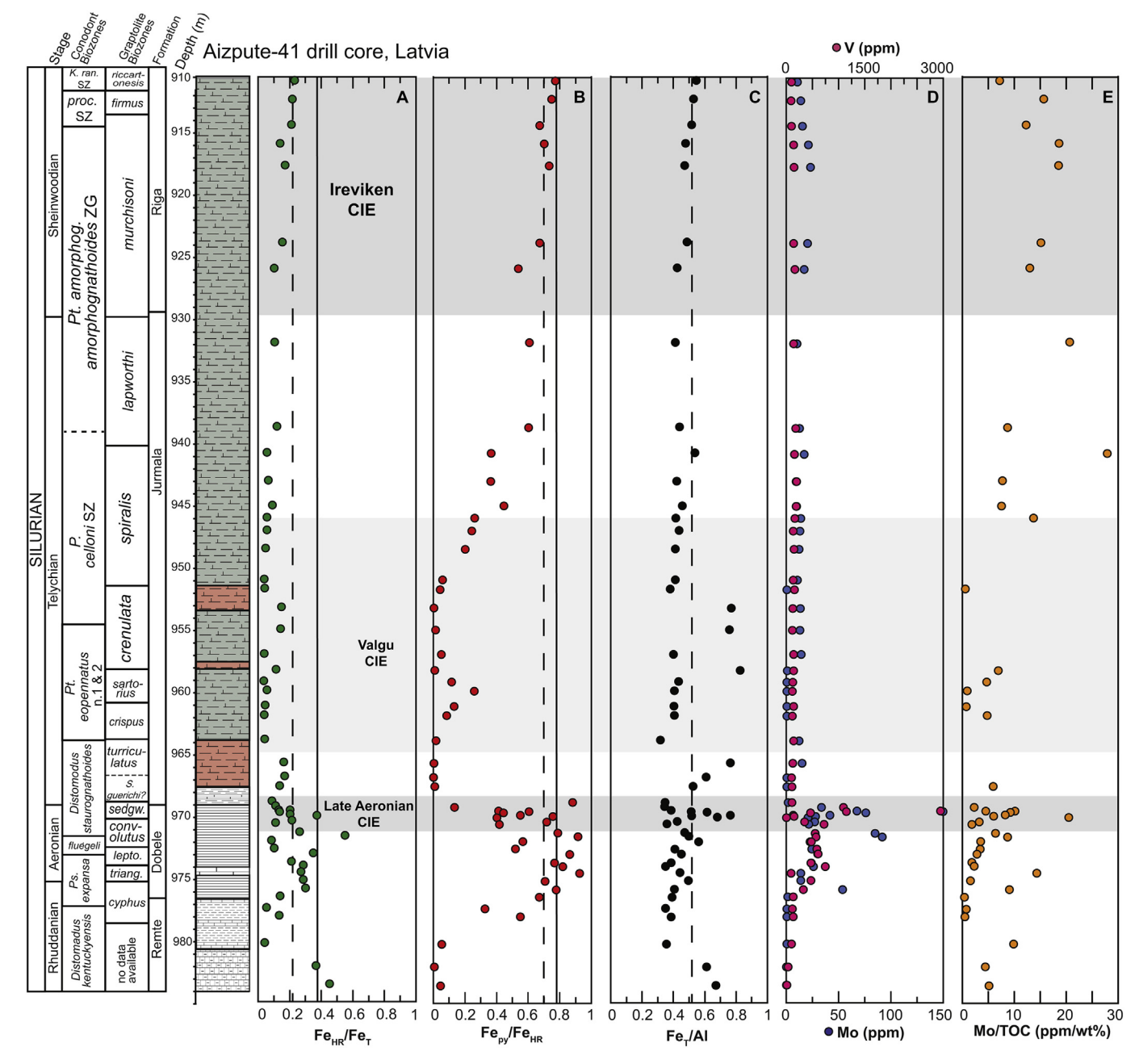


Fig. 5. Llandovery—early Wenlock (early Silurian) paleoredox geochemical data from organic-rich marls and mudstones of the Aizpute-41 drill core, Latvia. Grey bars denote globally documented positive carbon isotope excursions (CIEs). A, Dashed vertical line and solid line for Fe_{HR}/Fe_T represent the threshold for possibly anoxic (0.22) and anoxic (0.38) bottom waters, respectively. B, Dashed vertical line and solid line for Fe_{py}/Fe_{HR} represent the threshold for possibly euxinic (0.70) and anoxic (0.78) bottom waters, respectively. C, dashed vertical line represents Phanerozoic average crustal values for Fe_{Ty}/Al .

to the Dobele Formation black shales, Fe_{py}/Fe_{HR} values show enrichments towards values > 0.70. The Fe_{py}/Fe_{HR} values from the Dobele Formation are predominantly > 0.70 until the very top of the formation where they fall below 0.70. The Fe_{py}/Fe_{HR} values in the Jurmala Formation are generally low (below 0.70), but these values steadily increase towards the top *Monograptus firmus* graptolite biozone.

Molybdenum concentrations for the Aizpute-41 core overall are slightly enriched compared to modern oxic marine sediments with an average of 20 ppm (Figs. 5 and 6), however, the black shale facies of the Dobele Formation has an average of 45 ppm, ranging from 14 to 150 ppm. The most enriched molybdenum concentrations of 150 ppm correspond to Fe_{py}/Fe_{HR} values above 0.78 and coincide with peak $\delta^{13}C_{org}$ values in this upper Aeronian interval. The Mo concentrations within the Telychian Jurmala Formation average 8 ppm, with a range of

1 to 15 ppm. While molybdenum concentrations within the overlying early Wenlock Riga Formation increase to an average of 17 ppm, with a range from 10 to 23 ppm, corresponding to Fe_{HR}/Fe_{T} values below 0.38 and Fe_{pyr}/Fe_{HR} values below 0.70. Vanadium concentrations trend similarly to molybdenum concentrations throughout the Aizpute-41 core (Fig. 5D), with maximum vanadium concentrations of 3000 ppm corresponding to the interval with the elevated $\delta^{13}C_{org}$ values and highest molybdenum concentrations in the late Aeronian. Manganese concentrations and Mn/Al ratios show correlative trends throughout the Aizpute-41 core, with manganese concentrations predominantly below 850 ppm throughout the study interval and therefore were not plotted in Fig. 5 (see Appendix Table 2; Fig. DR1).

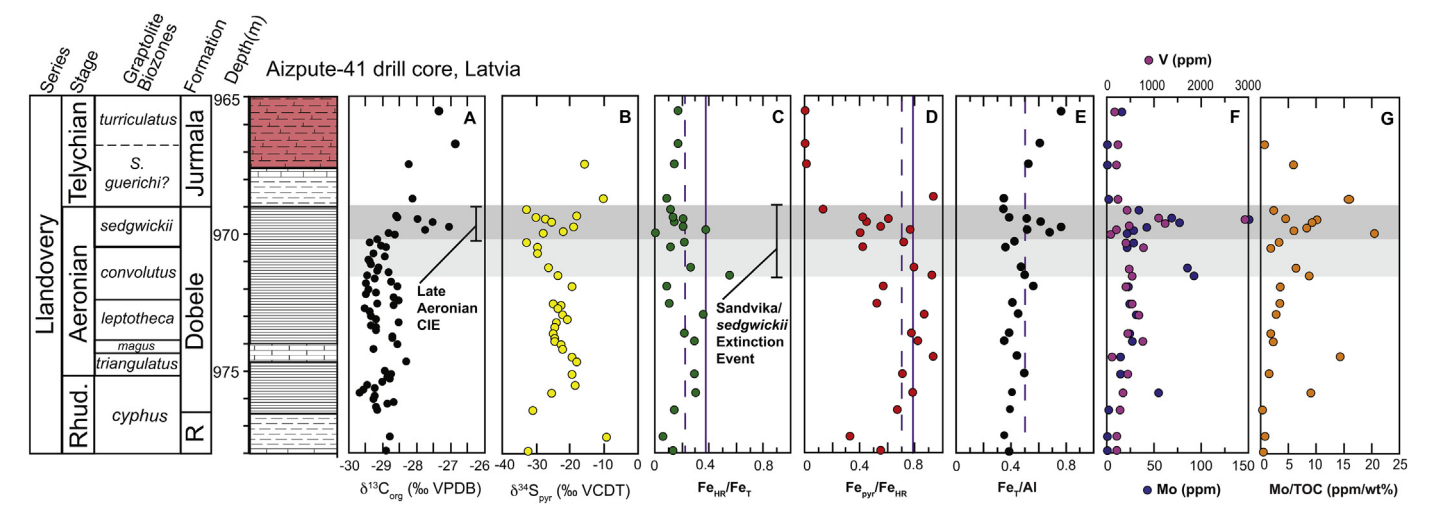


Fig. 6. Integrated Aeronian (early Silurian) geochemical data from the Aizpute-41 drill core, Latvia with the Sandvika/sedgwickii extinction records. Note that the light grey bar denotes the approximate range of the marine extinction interval based upon combined paleontological data (e.g., Cooper et al., 2014 and references therein), which begins before the Late Aeronian CIE (carbon isotope excusion–dark grey bar). Dashed and solid vertical lines are the same geochemical threshold levels for paleoredox data plotted in Fig. 5.

5. Discussion

Utilizing the previously detailed biostratigraphic studies of our two drill cores (see Section 2.1 above) allows us to constrain four globally documented CIEs from the Late Ordovician and early Silurian. The $+\,4\%$ magnitude perturbation in the Late Ordovician $\delta^{13}C_{\rm org}$ records from southern Sweden (Fig. 2) is documented as the global Hirnantian positive carbon isotope excursion or HICE (e.g., Bergstrom et al., 2016). The +2.5% magnitude perturbation in the $\delta^{13}C_{org}$ records from late Aeronian strata from both Aizpute-41 and Röstånga-1 cores (Figs. 2, 4, 6) have been documented as the globally occurring Late Aeronian CIE (e.g., Melchin and Holmden, 2006; Fryda and Storch, 2014). The early Telychian +2 to 2.5% magnitude perturbation in the $\delta^{13}C_{org}$ records from both Aizpute-41 and Röstånga-1 cores (Figs. 2 and 4) has been labeled as the globally recognized Valgu CIE (e.g., Munnecke and Mannik, 2009; Bancroft et al., 2015; Waid and Cramer, 2017). Lastly, the +2% magnitude perturbation in the $\delta^{13}C_{org}$ values from the late Telychian-early Sheinwoodian interval of the Aizpute-41 core (Fig. 4) is recognized as the rising limb of the Ireviken CIE, and correlates well with the positive perturbation in $\delta^{13}C_{\text{carb}}$ values previously documented from this drill core (Cramer et al., 2010).

Linear relationships between $\delta^{13}C_{org}$ values and TOC wt% can be indicative of diagenetic alteration through thermal heating or oxidative loss of volatile organic compounds (Meyers, 1994), which is particularly important for organic matter-rich facies such as those of the deep, basinal Röstånga-1 strata. Despite some degree of thermal heating suggested for the Röstånga-1 core (Bergström et al., 1999) these deeperwater black shales show no correlation between $\delta^{13}C_{org}$ and TOC wt% (R² = 0.04, $r \le 0.21, p > .01, n = 110$). The Aizpute-41 core samples show a low to moderate correlation between $\delta^{13}C_{org}$ and TOC wt% (R² = 0.38, r = 0.62, p < .0001, n = 112) which may be indicative of minimal amount of diagenetic or thermal alteration. Additionally, the CAI values for drill cores from this area of Latvia indicate these strata experienced even less thermal heating (CAI = 1; Nehring-Lefeld et al., 1997) than the Röstånga-1 core strata, thus it is unlikely that diagenetic alterations affected any of the reported data.

Here we interpret the broad-scale trends in our shale-based proxy data, Fe_{HR}/Fe_T, Fe_{py}/Fe_{HR}, and $\delta^{34}S_{py}$, to constrain local marine redox conditions (Figs. 3, 5, and 6). Subsequently, our local paleoredox interpretations help to constrain the global marine redox conditions of [Mo, V] which can record local redox conditions and/or global redox state of the ocean through the marine reservoir size (Gill et al., 2011a,

2011b; Reinhard et al., 2013; Sahoo et al., 2016; Owens et al., 2016).

Furthermore, constraining the redox conditions within the context of the known global biotic records for extinction/faunal turnover may provide a possible kill mechanism during these intervals. We focus on three intervals: latest Ordovician HICE, early Silurian Late Aeronian CIE, and early Silurian Ireviken CIE. The geochemical datasets from these intervals can be either a) compared to previously published paleoredox proxy data from time equivalent strata in the Baltic Basin or other basins, or b) these datasets document consistent trends from both study sections. The early Telychian shale-based redox proxy datasets from both study localities lack consistent trends, with only the southern Sweden section recording evidence for intermittent anoxic to possibly euxinic bottom water conditions based on elevated Fe_{HR}/Fe_T and Fe_{DV}/ Fe_{HR} during the Valgu CIE. Furthermore, there are no additional paleoredox records published through the early Telychian to compare to this dataset, thus there is no further paleoredox discussion on this interval as it remains underconstrained.

5.1. Late Ordovician HICE marine redox conditions and major mass extinction (LOME)

The Fe and trace metal geochemical records of the late Katian-Hirnantian organic-rich mudstones have previously been discussed (Hammarlund et al., 2012) from the nearby Billegrav-2 drill core (Bornholm Island, Denmark). Our study provides independent geochemical constraints on this deeper section of the Baltic Basin prior to, during, and after the HICE. The FeHR/FeT values of strata in the preexcursion through peak-HICE values interval (Fig. 3A) are consistent with modern marine sediments deposited under less reducing and possibly oxic water column conditions (Raiswell et al., 2018). However, in the late Hirnantian interval (falling limb of HICE and post-excursion baseline δ^{13} C values) Fe_{HR}/Fe_T values indicate anoxic conditions, while the corresponding Fe_{pv}/Fe_{HR} ratios trend from values less than the 0.7 euxinic threshold to more elevated values, supporting an interpretation of the local marine bottom waters becoming more reducing by the late Hirnantian. Reducing marine water column conditions (anoxic, ferruginous, and euxinic conditions) typically enrich Fe_T relative to Al (e.g., Raiswell et al., 2008). All Hirnantian samples record elevated Fe_T/Al values (compared to Paleozoic crustal average), but this is in contrast with corresponding lowered ratios of FeHR/FeT that suggest more oxic conditions. A possible explanation for the higher than expected Fe_T contents in the pre-excursion through peak-HICE interval is an elevated Fe delivery compared to Al that did not affect the Fe_{HR}/Fe_{T} ratio. This could be due to an enhanced silicate-Fe delivery to this area from glacioeustatic sea-level drop and subsequent increased continental weathering associated with Gondwana glaciation/ice sheet expansion during the Hirnantian. These trends in iron geochemistry are consistent with the previously published iron speciation data from the nearby Billegrav-2 drill core within the latest Katian through Hirnantian interval (Hammarlund et al., 2012). Overall these data are consistent with a weathering hypothesis that was previously proposed to explain both the HICE records and Gondwana glaciation at high latitudes (Kump et al., 1999).

Manganese concentrations from the HICE interval in the Röstånga-1 core. Sweden (Fig. 3F) are all well above the modern average for marine sediments deposited within an oxic water column conditions of ~850 ppm (Turgeon and Brumsack, 2006). Interestingly, [Mn] shows a significant enrichment trend from the pre-excursion through peak-HICE values interval coincident with increased carbonate content in these marine mudstones (i.e., a transition from siliciclastic mudstones to marls) and this is in the same interval where FeHR/FeT and FeDV/FeHR ratios increase to more reducing conditions (Fig. 3A,B,F). These corresponding Mn enrichments and Fepy/FeHR ratios could be due to increased amounts of reduced Mn-minerals deposited near a chemocline. This phenomenon is observed in the modern-day Black Sea where significant amounts of non-oxide Mn minerals, such as Mn-carbonates, are deposited as a "bathtub ring" near the chemocline where there is a mixing of anoxic waters with overlying oxic waters (Force and Cannon, 1988; Force and Maynard, 1990; DeLange et al., 2008). Subsequently, Mn contents decrease abruptly to values well below the modern marine oxic threshold within the late Hirnantian black shales in the post-HICE baseline interval. Vanadium concentrations, a trace-metal proxy that requires low-oxygen to an anoxic water column, but not necessarily euxinic conditions (e.g., Algeo and Maynard, 2004; Sahoo et al., 2012, 2016; Reinhard et al., 2013; Owens et al., 2016, 2017) also show mildly enriched values in these late Hirnantian black shales. However, Mo contents, which require euxinic conditions to enrich significantly (20 to > 100 ppm), show only minimal enrichments in this interval despite Fe speciation evidence for sulfidic conditions. These muted Mo enrichments within the late Hirnantian black shales are consistent with modern non-euxinic water columns that have sulfide restricted to sediment porewaters (Hardisty et al., 2018). This interval of minor enrichments [V, Mo] documented here is consistent with the modest Mo enrichments (~25 ppm) documented from the late Hirnantian interval within nearby Billegrav-2 core (Hammarlund et al., 2012). Therefore, both trace metals and Fe speciation suggest only a local to regional shift from oxic conditions to a reducing marine water column from the early to late Hirnantian. These elevated Fe_{HR}/Fe_{T} and Fe_{py}/Fe_{HR} ratios combined with modest enrichments of [Mo] could potentially be the result of a drawdown of marine trace metal inventories in the latest Hirnantian oceans (see below for further global redox discussion).

Global biotic records from late Katian through Hirnantian document a major mass extinction event, the LOME, historically shown to be composed of two distinct pulses (Brenchley et al., 1994, 2001), although a single pulse has been recently proposed (Wang et al., 2019). The first pulse of extinction mainly affected nektonic and planktonic organisms in the shallow shelf and some deeper water environments, while the second pulse impacted faunas across a wide range of marine habitats (Harper et al., 2014). Finnegan et al. (2012) have argued for global cooling and habitat loss as major drivers for extinction in lowlatitude settings. Euxinia has also been proposed as the main driver for both pulses of the LOME, however support for this mechanism is largely based upon local redox proxy evidence from a few low-latitude marine basins (e.g., Zou et al., 2018). Our local redox proxies, Fe speciation and trace metal data, along with the correlative data of Hammarlund et al. (2012) suggest that marine environments were locally to regionally oxic within the Baltic Basin during the latest Katian and into the earlymid Hirnantian, coincident with the rising limb and peak $\delta^{13} C$ values of the HICE. This shift to more oxic marine conditions into the early Hirnantian from the late Katian has also been recorded in shale geochemical records from the Carnic Alps, Austria and Dobs Linn, Scotland (Hammarlund et al., 2012). Shale redox proxy records from South China show evidence for euxinic conditions during both pulses of the LOME, however, the extent of reducing conditions in this basin decreased from the pre-HICE to peak-HICE values interval (Zhang et al., 2009; Yan et al., 2012; Zou et al., 2018). These trends in local paleoredox proxy records from multiple ocean basins also coincide with continued eustatic sea-level fall as ice sheets over Gondwana reached their maximum extent during the Hirnantian (e.g., Brenchley et al., 2006; Harper et al., 2014). Thus, as global temperatures declined and eustatic sea-level fell, many of the remaining marine settings became more ventilated with oxic to suboxic conditions.

Additionally, δ34S_{CAS} records (a global paleoredox proxy) and geochemical modeling have shown that Hirnantian $\delta^{34}S_{pv}$ records (a local paleoredox proxy) are more reflective of changes in MSR-related sulfur isotopic fractionation associated with global cooling and glaciation at this time, and not changes in global increases in pyrite burial under widespread euxinic conditions (Jones and Fike, 2013; Present et al., 2015). A recent study has linked glacioeustatic sea-level change to large variations in $\delta^{34}S_{py}$ records from marine sediments deposited over the last 500 kyr, whereby positive excursions in $\delta^{34}S_{py}$ are driven by changes in sedimentation rates and connectivity with overlying water column during sea-level fall (Pasquier et al., 2017). Therefore, combining the interpretations of our data with previous publications suggest that the mechanism for the first extinction pulse of the LOME involved a major eustatic sea-level drop of ≥100 m, global cooling, and glaciation. Glacioeustatic sea-level drawdown would have drained widespread epeiric seaways globally, thus eliminating vast areas of habitable shallow marine environments in the Hirnantian (Sheehan, 2001). This dramatic reduction in marine shelf area would have led to the extinction of many endemic communities via habitat loss and carrving capacities of the remaining environments being exceeded (Brenchley et al., 2001). Recent sea-level reconstructions from sedimentary successions on Baltica, including both Aizpute-41 and Röstånga-1drill cores, suggest multiple regressive events within the Hirnantian (Kiipli and Kiipli, 2020). Sea-surface temperature proxies record a rapid cooling by ~5 °C during the Hirnantian and are consistent with this climate-driven first extinction pulse scenario (Trotter et al., 2008; Finnegan et al., 2011).

Global temperatures and eustatic sea level rose during the late Hirnantian, and local paleoredox proxy records (i.e., Fe speciation and trace metals) from multiple ocean basins indicate that anoxic marine conditions were widespread on continental margins at this time (Finnegan et al., 2011; Hammarlund et al., 2012; Melchin et al., 2013; Ahm et al., 2017; Zou et al., 2018). Additionally, the [Mo] vs. TOC values from the late Hirnantian in the southern Sweden section (Fig. 3E; Fig. DR1) covary with minor trace metal enrichments. The relationship of [Mo] to TOC wt% from modern and ancient euxinic marine conditions is well-documented, and this relationship can vary depending upon basins connectivity to the open ocean which affects the overall basin Mo inventory budget (Lyons et al., 2009). The Mo/TOC values for the pre-HICE to peak-HICE values interval are largely near zero with several intervals of high values (20 to 40) that are largely reflective of low [Mo] relative to even lower TOC contents (< 0.2%), and not of values consistent with modern euxinic basins. The elevated Mo/TOC values (average of 7.3) in the falling limb and post-HICE baseline interval (Fig. 3D, E) and the corresponding minor trace metal enrichments could be the result of either a semi-restricted basin or possibly global drawdown of marine trace metal inventories. If trace metal enrichments in this basin during the latest Ordovician were primarily controlled by weak connectivity with the adjacent Iapetus Ocean and thus the renewal times of deep basinal waters were greater than rates of Mo uptake this would be similar to Mo-depleted modern Black Sea and Framvaren Fjord that have comparable Mo/TOC values (~4.5 to 9;

Algeo and Lyons, 2006). The other possibility is that latest Ordovician trends in trace metals and Mo/TOC resulted from a global drawdown of marine trace metal inventories due to an expansion of euxinia during the latest Hirnantian on the order of that suggested for the Cretaceous Oceanic Anoxic Event 2 (OAE2; Owens et al., 2016; Dickson, 2017). Due to the limited amount of high-resolution Hirnantian trace metal datasets we cannot confidently interpret our trends as being the result of a global expansion of euxinia at this time.

Our local dataset from southern Sweden, when combined with other studies from several basins within the late Hirnantian, indicates these local environments were euxinic and these conditions persisted through the early Rhuddanian (Hammarlund et al., 2012; Zou et al., 2018). However, there is no observed positive excursion in $\delta^{34}S_{CAS}$ values (Jones and Fike, 2013) which would be expected for a global expansion of euxinia that coincided with these observed local paleoredox shifts as has been observed for other Phanerozoic events (Gill et al., 2011a, 2011b; Owens et al., 2013; Young et al., 2019). A recently generated $\delta^{238} \text{U}$ record from Hirnantian marine carbonates (same succession previously analyzed for δ³⁴S_{CAS} records), indicates that anoxic conditions increased globally and were a potential kill mechanism for the second pulse of the LOME (Bartlett et al., 2018). When combining both global and local paleoredox proxy records throughout the late Hirnantian interval they suggest an expansion of non-sulfidic anoxia in the global oceans, likely within continental margin settings, may have been a causal mechanism for the second extinction pulse of the LOME.

5.2. Late Aeronian CIE (early Silurian) marine redox conditions, marine extinction (Sandvika/sedgwickii event), and widespread anoxia

The Röstånga-1 core, Sweden and Aizpute-41 core, Latvia represent distinct marine depositional environments, and the similarities between iron and trace metal geochemistry, particularly in the late Aeronian strata, suggest primary signatures that are indicative of at least regional to potentially global redox conditions. The majority of the Fe_{HB}/Fe_T values from the late Aeronian interval of the Kallholn Formation in Sweden (Fig. 3A) and Dobele Formation in Latvia (Fig. 6C) are enriched relative to average modern oxic marine sediments suggesting that there was an expansion of anoxic conditions prior to and during peak values of the Late Aeronian CIE (Raiswell et al., 2018). The corresponding Fe_{DV}/Fe_{HR} ratios before the Late Aeronian CIE document values greater than the 0.7 euxinic threshold, and trend towards less enriched values through the duration of the CIE interval, suggesting the local conditions were initially very reducing (i.e., sulfidic) and shifted towards more oxic conditions. The Fe_T/Al ratios within this same interval at the Sweden locality show a trend from values within the Phanerozoic crustal averages (e.g., Raiswell et al., 2008) to values that are notably enriched in iron relative to aluminum. A local shift to a more reducing water column is not necessarily favored for the observed enrichment in Fe_T/Al ratio at the Sweden locality as Fe speciation data indicate a shift to more oxic marine waters. A possible explanation for the trend to significantly enriched Fe_T contents through the Late Aeronian CIE interval is more likely related to an elevated detrital Fe_T/Al ratio as sea level began to drop at this time in the Baltic Basin (Johnson, 2010). However, the Fe_T/Al values from Latvia show a different trend where ratios are at or slightly below Phanerozoic crustal averages in the pre-Late Aeronian CIE interval, and then increase to enriched Fe_T/Al ratios that closely correspond to the CIE. These distinct trends in Fe_T/Al values suggest a more enhanced Fe transport and trapping by locally euxinic conditions and associated Fe scavenging through local pyrite formation. This is consistent with the corresponding $\delta^{34}S_{py}$ data from both Sweden and Latvia which record a + 14‰ to +22‰ magnitude shift indicating a local to regional increase in pyrite burial (Figs. 2 and 6). Coincident parallel positive excursions in $\delta^{34}S_{pv}$ and $\delta^{13}C$ records have also been documented in many intervals throughout the Paleozoic in association with widespread reducing conditions and marine extinction - for example, the late Cambrian SPICE (Gill et al., 2011a,

2011b), Early Ordovician (Tremadocian; Edwards et al., 2018), early Silurian (Ireviken CIE; Rose et al., 2019; Young et al., 2019), and late Silurian (Lau CIE; Bowman et al., 2019). When our late Aeronian $\delta^{13} C$ and $\delta^{34} S_{py}$ excursion records are interpreted together with Fe speciation and trace metal (see discussion below) datasets they are consistent with a transient increase in global burial rates of reduced carbon and sulfur species.

A notable extinction event in late Aeronian strata has been documented among many taxa from the early Silurian oceans, known as the 'Sandvika Event' (e.g., Jeppsson, 1998). It has been estimated that ~23% of conodont and trilobite species became extinct, while brachiopods and acritarchs (microphytoplankton) also show evidence for significant turnover and extinction (Helbert et al., 1982; Thomsen and Baarli, 1982; Chatterton et al., 1990; Aldridge et al., 1993; Jeppsson, 1998). Additionally, there was a major extinction in graptolites (a major Paleozoic zooplankton group) at this time, spanning the late L. convolutus and S. sedgwickii graptolite biozones (Storch, 1995; Melchin et al., 1998; Cooper et al., 2014; Crampton et al., 2016). These biotic records can now be integrated with our new $\delta^{13}\text{C}$ datasets from Baltica that documents a correlation of the Late Aeronian CIE with the Sandvika/sedgwickii events. Specifically, the onset of the extinction event is now shown to precede the Late Aeronian CIE (Fig. 6). Marine fauna representative of both shallow- and deep-water environments are documented to have correlative extinctions during the same interval that geochemical evidence suggests an expansion of reducing bottom water conditions. However, these observations combined with our new geochemical data indicate that these marine taxa were affected by the same event and potential mechanism that caused the perturbation to the global carbon cycle.

The new Fe speciation and trace metal geochemical records suggest anoxic to euxinic bottom water conditions were present, at least, in the southwestern and eastern portions of the Baltic Basin during the late Aeronian (Fig. 7). Additionally, previously published shale-proxy data from the Kallholn Formation in the northern part of the Baltic Basin also indicates reducing marine conditions (Lu et al., 2017), and these strata are broadly correlative to our Late Aeronian sections (Bergström et al., 2012; Walasek et al., 2018). Specifically, there are two intervals of [V, Mo] enrichments of up to 3000 and 150 ppm, respectively, followed by drawdowns within the Sandvika/sedgwickii extinction interval. The first trace metal enrichment-drawdown trend occurs in the pre-Late Aeronian CIE interval, and a second that occurs within the CIE interval (Figs. 3 and 6). Additionally, [Mo] to TOC values from both sections covary with the trace metal enrichment and drawdown trends allowing for potential reservoir relationships to be assessed as corresponding Fe speciation data suggest relatively stable euxinic conditions at both study sites (Figs. 3 and 6). Mo/TOC data from pre-Late Aeronian CIE interval from both sections average between 7.5 and 12.4, and then these values enrich to average values of 20.5 to 23.7 for the two sections within the Late Aeronian CIE (Figs. 3E and 6G). After both of the intervals of high Mo/TOC ratios the values decline to averages of \leq 2.5. The declines in [V, Mo] and corresponding changes in Mo/TOC could be suggestive of a global expansion of reducing conditions prior to and during the Late Aeronian CIE, whereby expansion of reducing conditions would have depleted marine inventories of redox-sensitive metals.

Dramatic declines in trace metal concentrations have been associated with OAE2 where the global drawdown of [V] preceded the CIE while [Mo] drawdown occurred nearly coincided with the OAE (defined by the CIE), however, the locality distinguishing this stratigraphic framework was at a very high-resolution (e.g., Owens et al., 2016, 2017). Importantly, model estimates suggest only 3 to 7% of the seafloor experienced euxinic conditions during OAE2 (Owens et al., 2013, 2016; Dickson, 2017), thus ocean-scale reducing conditions are necessary for the documented trace metal drawdowns. These patterns of trace metal concentrations and Mo/TOC dynamics could also reflect the strength of the Baltic Basin's connectivity to the Iapetus Ocean during the late Aeronian, and thus the renewal time of this basin's deep waters

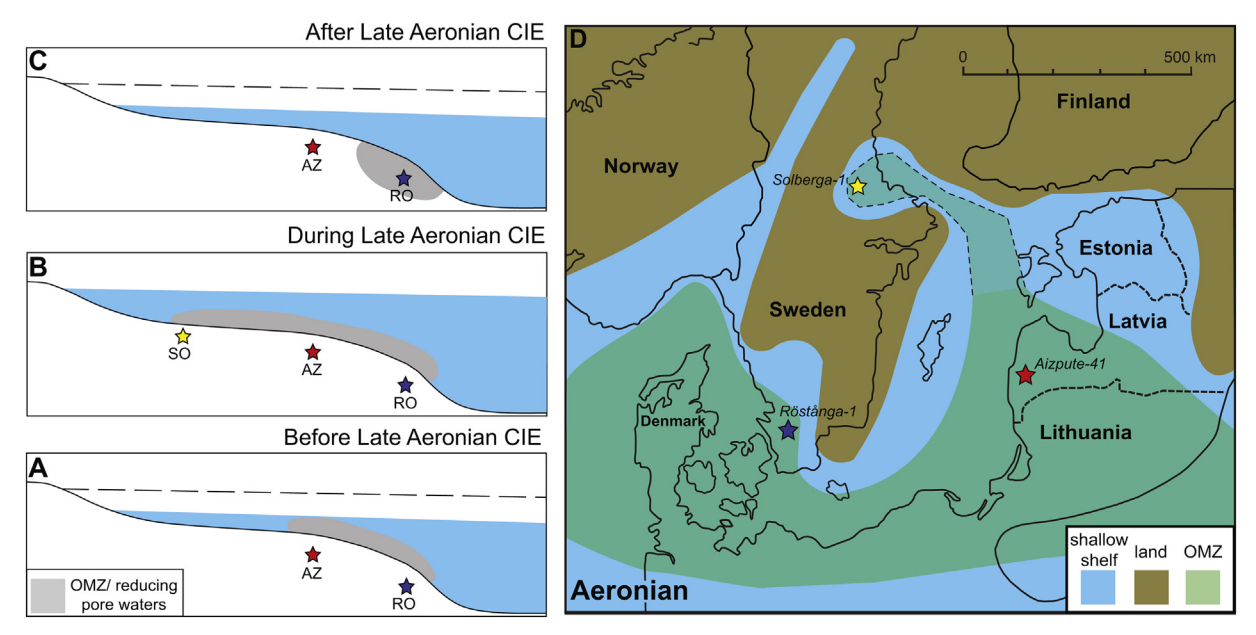


Fig. 7. Conceptual model of marine redox changes in the Baltic Basin during the late Aeronian. A, Cross section illustrating an oxygen minimum zone (OMZ) before the Late Aeronian CIE across the Baltic Basin shelf to slope transect. Changes in sea level (relative to sea-level highstand during the Late Aeronian CIE in panel-B are shown by a dashed line. B, Cross section illustrating an expanded OMZ during the Late Aeronian CIE across the Baltic Basin shelf to basin transect. C, Cross section illustrating presence of sulfide in sediment pore waters after the Late Aeronian CIE across the Baltic Basin shelf to slope transect. D, Map-view schematic illustrating the maximum aerial extent of the OMZ in the Baltic Basin during sea-level rise in the late Aeronian. Solid black line indicates the extent of OMZ based on redox data from this study. Dashed black line indicates possible extent of OMZ based on redox data from the Solberga-1 drill core (Lu et al., 2017). SO: Solberga-1 core; AZ: Aizpute-41 core; RO: Röstånga-1 core.

relative to Mo uptake rates and sulfide build-up within the water column as Mo/TOC ranges from averages near modern Framvaren Fjord (\sim 9) to values within the modern range of Cariaco Basin (\sim 25; Algeo and Lyons, 2006). These patterns of marine redox dynamics are consistent with eustatic sea-level rise (i.e., Haq and Schutter, 2008; Johnson, 2010) that could have caused an expansion of anoxic and euxinic waters from deeper marine environments into shallower shelf settings as a causal mechanism for the extinction event and associated global perturbation of the carbon cycle (Fig. 8). Furthermore, our data suggest at least regional expansion of anoxia to euxinia preceded the Late Aeronian CIE and coincided with the onset of the extinction, a pattern that has been recently documented for the late Silurian Lau CIE and the associated progression of the extinction event (Bowman et al., 2019) and at least two Mesozoic OAEs (Ostrander et al., 2017; Them et al., 2018). However, to confidently attribute our late Aeronian trace metal drawdowns to either global depletion of marine inventories or local basinal factors related to eustatic sea-level and open ocean connectivity, further studies are required to confirm this hypothesis from additional ocean basins that were persistently euxinic before, during, and after the Late Aeronian CIE and/or utilizing a redox proxy that is more indicative of global processes.

5.3. Ireviken CIE (early Silurian) marine redox conditions, marine extinction (Ireviken Event) and widespread anoxia

This study provides the first shale-based redox proxy data spanning the Llandovery-Wenlock boundary and the rising-limb of the associated Ireviken CIE. Our Fe speciation and Fe_T/Al ratios indicate a transition to increasingly reducing marine water column conditions leading into the rising limb of the Ireviken CIE. The corresponding $\delta^{34}S_{py}$ data from this interval of the Aizpute-41 core, Latvia record a + 13% magnitude excursion that is coincident with the rising limb of the Ireviken CIE (Fig. 4), indicating a local increase in pyrite burial, consistent with Fe speciation data (Fig. 5A-C) indicating a shift to more locally reducing conditions. This positive excursion in $\delta^{34}S_{py}$ data can also be seen in carbonate sections within the Baltic Basin (Richardson et al., 2019;

Rose et al., 2019) and the Great Basin, Nevada suggesting a more global extent of reducing conditions and an overall increase in pyrite burial rates (Young et al., 2019). The [Mn] concentrations for the upper Jurmala-lower Riga formations (data repository Table 2) are all well below the average shale values suggestive of locally reducing conditions. Vanadium concentrations only show minimal enrichments (average of 150 ppm) across the upper Jurmala-lower Riga formations (Fig. 5D), and then a steady decline through the rising limb of the Ireviken CIE. Molybdenum contents show modest enrichments (average of 20 ppm) and a decline over the same interval as vanadium, with enrichments overlapping with modern marine environments that are intermittent/seasonally euxinic (Scott and Lyons, 2012). When we combine these [Mo] with the corresponding Fe speciation data it suggests that sulfidic conditions were likely limited to the sediment porewaters or very close to the sediment-water interface.

The Ireviken Event is recorded within late Llandovery-early Wenlock strata (Fig. 4), and is one of the most severe marine extinction events of the Silurian which has been documented globally (e.g., Calner, 2008). Most marine clades were affected by this extinction event, including severe declines in conodonts, graptolites, trilobites, acritarchs, chitinozoans, corals, and brachiopods (e.g., Jeppsson, 1997; Melchin et al., 1998; Munnecke et al., 2003; Hints et al., 2018). These early Silurian paleontological records of global biotic change have been previously well-integrated with $\delta^{13}C$ datasets that document an associated positive shift, the Ireviken CIE (e.g., Cramer et al., 2010). Furthermore, recent carbonate-based paleoredox studies have shown direct evidence, from multiple basins and paleocontinents, for both local and global expansion of reducing conditions throughout this marine extinction event and associated CIE (Richardson et al., 2019; Rose et al., 2019; Young et al., 2019). Both Fe and trace metal concentrations from the western Latvia section provide evidence for a shift towards more reducing conditions in this deep shelf setting of the Baltic Basin (Fig. 5A-D). Although [Mn] are low throughout the late Llandoveryearly Wenlock boundary interval, iron speciation values shift from oxic to possibly anoxic/euxinic conditions during the rising limb of the Ireviken CIE (Fig. 5A-B). Additionally, Mo/TOC ratios from this section

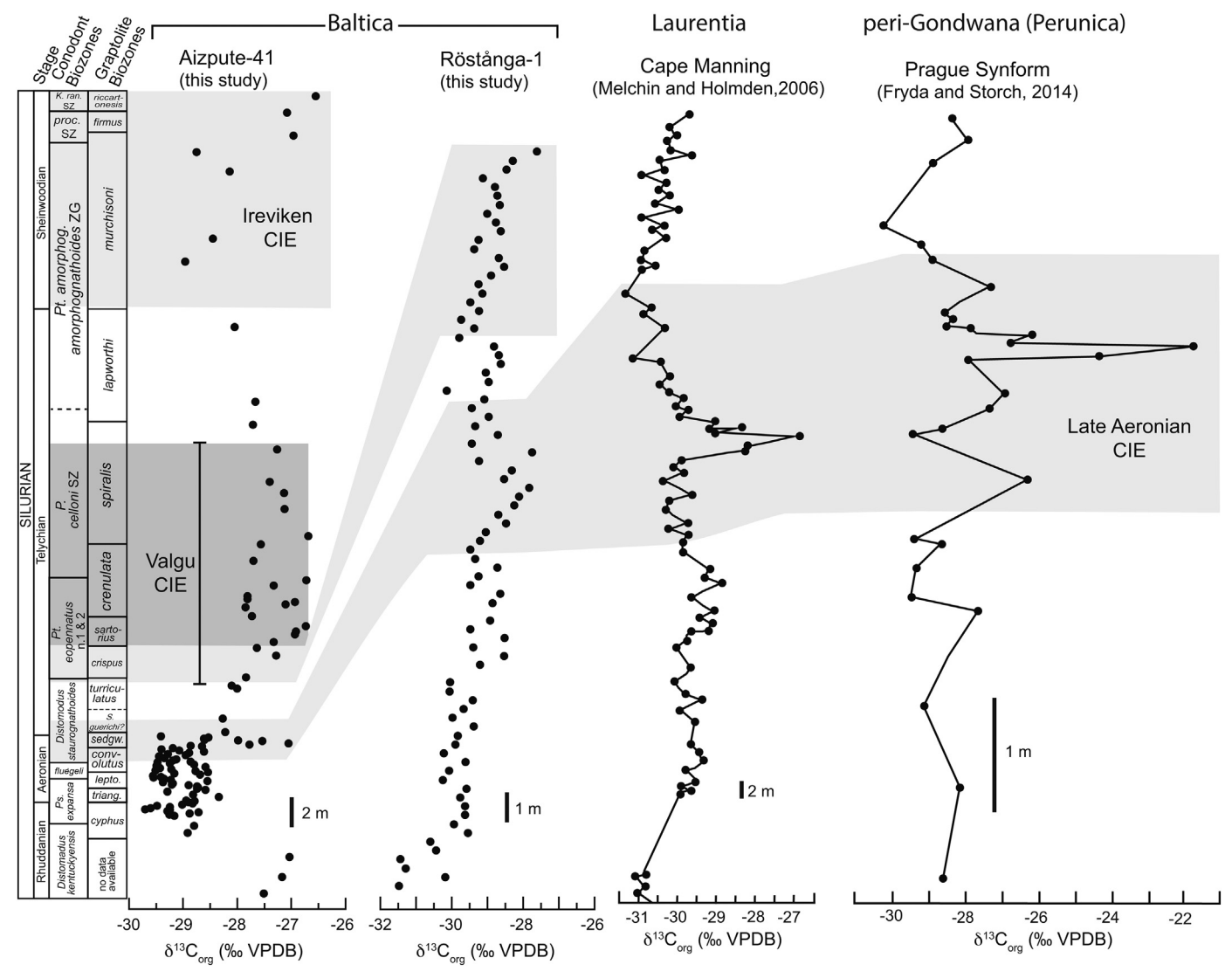


Fig. 8. Correlation of $\delta^{13}C_{org}$ data between sections from Baltica sections (this study), Laurentia (Melchin and Holmden, 2006), and peri-Gondwana (Perunica terrane; Fryda and Storch, 2014). Please note that positions of grey boxes indicate intervals of strata at each section that can be confidently correlated using graptolite biostratigraphy and now $\delta^{13}C_{org}$ chemostratigraphic profiles. The boundaries of the grey boxes for the Late Aeronian CIE and Valgu CIE scale with thickness and relative position of graptolite biozone boundaries within each of the sections.

covary with the trace metal enrichment and possible drawdown, with average values ~17.5 in the lower Riga Formation that then trend to values of 7.2 (Fig. 5E). Similar to the previous late Aeronian trace metal discussion (Section 5.2 above), this could represent a potential early Wenlock trace metal drawdown. The corresponding change in Mo/TOC values possibly suggesting a global expansion of reducing conditions that began to deplete the marine inventories of redox-sensitive metals or, conversely, changes in basin connectivity to the open ocean during the Ireviken CIE. Sea-level records across this interval broadly indicate a rise in the early Wenlock (Johnson, 2010). However, detailed sealevel reconstructions from the nearby Priekule core, Latvia together with evidence from other Baltic sections indicate that the uppermost sampled part in the Aizpute-41 core corresponds to a sea-level lowstand (Kiipli et al., 2010). This is consistent with basin restriction explanation of trace metal and Mo/TOC records documented here. However, further exploration is required from different sections and basins that were persistently euxinic before, during, and after the Ireviken CIE.

6. Conclusions

The documented stratigraphic trends in geochemical data from

deeper marine settings of southern Sweden (Röstånga-1 core) and western Latvia (Aizpute-41 core) feature dynamic local and potentially global marine redox conditions surrounding the latest Ordovician HICE, Late Aeronian CIE, and Ireviken CIE and associated extinction events. The new late Katian-Hirnantian shale-based redox proxy data, FeHR/ Fe_T, Fe_{pv}/Fe_{HR}, and [V, Mo], suggest a perturbation from oxic to anoxic bottom water conditions with a local to regional extent that occurred during the late Hirnantian, but did not coincide with the peak δ^{13} C values (HICE) and correlative positive $\delta^{34}S_{py}$ excursion. Furthermore, when combining these new geochemical datasets with previously published local and global paleoredox studies, it suggests that an expansion of non-sulfidic anoxia in the global oceans may have been a causal mechanism for the second extinction pulse of the LOME during late Hirnantian sea-level rise and deglaciation. However, additional redox proxy application is required to continue assessing the role of marine redox conditions played in the first major mass extinction event of the Phanerozoic.

Our integrated Fe speciation, trace metal, $\delta^{13}C_{\rm org}$, and $\delta^{34}S_{\rm py}$ datasets are some of the first to constrain local to regional marine redox conditions within the Baltic Basin throughout the Llandovery. The new shale-based redox proxies from two sections show evidence for anoxic

to euxinic water column conditions across this basin prior to, and during the Late Aeronian CIE. Additionally, there are two intervals of trace metal enrichment followed by drawdowns within the upper Aeronian strata, and these could be linked to either global depletion of marine inventories or local basinal factors related to eustatic sea-level and open ocean connectivity. Further studies are required from a different basin with persistently euxinic conditions to assess the ultimate causes of these trends in trace metal data. Regardless, these new shalebased multiproxy datasets reveal strong evidence for at least regional expansion of water column anoxic to euxinic conditions, and possibly on a global scale. Our new late Aeronian $\delta^{13}C_{org}$ and $\delta^{34}S_{py}$ records show parallel positive excursions indicating that increased burial of organic carbon and pyrite under widespread anoxic to euxinic conditions occurred during this time. These geochemical trends are consistent with an expansion of anoxic to locally euxinic waters from deeper marine environments into shallower shelf settings as a causal mechanism for the associated marine extinction events (Sandvika/ sedgwickii events). Lastly, our late Llandovery-early Wenlock shalebased redox proxy data document enrichments that suggest anoxic to intermittent euxinic bottom water conditions were coincident with the rising limb of the Ireviken CIE in the deeper shelf setting of Latvia. These data are consistent with previous carbonate-based redox proxy studies that suggest that the Ireviken CIE and associated marine extinction represents one of many major anoxic-euxinic events in Late Ordovician-Silurian oceans. More broadly, our study supports previous studies of oxygen depletion in subsurface waters of Paleozoic oceans and highlights oxygen's critical role in biospheric evolution in the early Paleozoic.

Acknowledgments

Ted Present and one anonymous reviewer are thanked for their constructive reviews that helped improve this paper and Cole Edwards and Tom Algeo for editorial direction. This study was funded by the American Chemical Society Petroleum Research Fund (grant ACS-PRF#57487-DNI2 to S.A.Y.) and the National Science Foundation (EAR-1748635 to S.A.Y. and J.D.O.). O'H and T.M acknowledge support from the Estonian Research Council (grants PRG836 and PUT611). We thank Mats Eriksson and Per Ahlberg for assistance with sampling of the Röstånga-1 core at Lund University. Additionally, we thank Burt Wolff and John Khawam for assistance with geochemical analyses at Florida State University. All geochemical work was performed at the National High Magnetic Field Laboratory, which is supported by the National Science Foundationa Cooperative Agreement No. DMR-1157490 and the State of Florida.

Appendix A. Supplementary data

Supplementary data to this article can be found online at https://doi.org/10.1016/j.palaeo.2020.109792.

References

- Ahm, A.S.C., Bjerrum, C.J., Hammarlund, E.U., 2017. Disentangling the record of diagenesis, local redox conditions, and global seawater chemistry during the latest Ordovician glaciation. Earth Planet Sci. Lett. 459, 145–156.
- Aldridge, R.J., Jeppsson, L., Dorning, K.J., 1993. Early Silurian Oceanic Episodes and events. J. Geol. Soc. Lond. 150, 501–513.
- Algeo, T.J., 2004. Can marine anoxic events draw down the trace element inventory of seawater? Geology 32, 1057–1060.
- Algeo, T.J., Lyons, T.W., 2006. Mo-total organic carbon covariation in modern anoxic marine environments: Implications for analysis of paleoredox and paleohydrographic conditions. Paleoceanography 21.
- Algeo, T.J., Maynard, J.B., 2004. Trace-element behavior and redox facies in core shales of Upper Pennsylvanian Kansas-type cyclothems. Chem. Geol. 206, 289–318.
- Algeo, T.J., Maynard, J.B., 2008. Trace-metal covariation as a guide to water-mass conditions in ancient anoxic marine environments. Geosphere 4, 872–887.
- Algeo, T.J., Tribovillard, N., 2009. Environmental analysis of paleoceanographic systems based on molybdenum-uranium covariation. Chem. Geol. 268, 211–225.

- Bancroft, A.M., Brunton, F.R., Kleffner, M.A., 2015. Silurian conodont biostratigraphy and carbon (delta C-13(carb)) isotope stratigraphy of the Victor Mine (V-03-270-AH) core in the Moose River Basin. Can. J. Earth Sci. 52, 1169–1181.
- Bartlett, R., Elrick, M., Wheeley, J.R., Polyak, V., Desrochers, A., Asmerom, Y., 2018.
 Abrupt global-ocean anoxia during the late Ordovician-early Silurian detected using uranium isotopes of marine carbonates. P Natl. Acad. Sci. USA 115, 5896–5901.
- Bergström, S.M., Huff, W.D., Koren, T., Larsson, K., Ahlberg, P., Kolata, D., 1999. The 1997 core drilling through Ordovician and Silurian strata at Röstånga, S. Sweden: preliminary stratigraphic assesment and regional comparison. GFF 121, 127–135.
- Bergström, S.M., Eriksson, M.E., Young, S.A., Widmark, E.-M., 2012. Conodont biostratigraphy, and 813C and 834S isotope chemostratigraphy, of the uppermost Ordovician and lower Silurian at Osmundsberget, Dalarna, Sweden. Gff 134, 251-272.
- Bergstrom, S.M., Eriksson, M.E., Schmitz, B., Young, S.A., Ahlberg, P., 2016. Upper Ordovician delta C-13(org) chemostratigraphy, K-bentonite stratigraphy, and biostratigraphy in southern Scandinavia: a reappraisal. Palaeogeogr. Palaeocl. 454, 175-188
- Berner, R.A., 1985. Sulfate Reduction, Organic-Matter Decomposition and Pyrite Formation. Philos. T R Soc. A 315, 25–38.
- Berner, R.A., 2006. GEOCARBSULF: a combined model for Phanerozoic atmospheric O-2 and CO2. Geochim Cosmochim Ac 70, 5653–5664.
- Bickert, T., Patzold, J., Samtleben, C., Munnecke, A., 1997. Paleoenvironmental changes in the Silurian indicated by stable isotopes in brachiopod shells from Gotland, Sweden. Geochim Cosmochim Ac 61, 2717–2730.
- Bjerreskov, M., Jørgensen, K.Å., 1983. Late Wenlock graptolite bearing tuffaceous sandstone from Bornholm, Denmark. Bull. Geol. Soc. Den. 31, 129–149.
- Bowman, C.N., Young, S.A., Kaljo, D., Eriksson, M.E., Them, T.R., Hints, O., Martma, T., Owens, J.D., 2019. Linking the progressive expansion of reducing conditions to a stepwise mass extinction event in the late Silurian oceans. Geology 47, 968–972.
- Boyer, D.L., Owens, J.D., Lyons, T.W., Droser, M.L., 2011. Joining forces: combined biological and geochemical proxies reveal a complex but refined high-resolution palaeo-oxygen history in Devonian epeiric seas. Palaeogeogr. Palaeocl. 306, 134-146.
- Brenchley, P.J., Marshall, J.D., Carden, G.A.F., Robertson, D.B.R., Long, D.G.F., Meidla, T., Hints, L., Anderson, T.F., 1994. Bathymetric and Isotopic evidence for a Short-Lived late Ordovician Glaciation in a Greenhouse Period. Geology 22, 295–298.
- Brenchley, P.J., Marshall, J.D., Underwood, C.J., 2001. Do all mass extinctions represent an ecological crisis? Evidence from the late Ordovician. Geol. J. 36, 329–340.
- Brenchley, P.J., Marshall, J.D., Harper, D.A.T., Buttler, C.J., Underwood, C.J., 2006. A late Ordovician (Hirnantian) karstic surface in a submarine channel, recording glacioeustatic sea-level changes: Meifod, Central Wales. Geol. J. 41, 1–22.
- Bruchert, V., Pratt, L.M., 1996. Contemporaneous early diagenetic formation of organic and inorganic sulfur in estuarine sediments from St Andrew Bay, Florida, USA. Geochim Cosmochim Ac 60, 2325–2332.
- Calner, M., 2008. Silurian global events-at the tipping point of climate change. In: Ashraf, M.T. (Ed.), Mass Extinctions. Springer-Verlag, Berlin and Heidelberg, pp. 21–58.
- Canfield, D.E., Raiswell, R., Bottrell, S., 1992. The Reactivity of Sedimentary Iron Minerals toward Sulfide. Am. J. Sci. 292, 659–683.
- Chatterton, B.D.E., Edgecombe, G.D., Tuffnell, P.A., 1990. Extinction and Migration in Silurian Trilobites and Conodonts of Northwestern Canada. J. Geol. Soc. Lond. 147, 703–715.
- Cocks, L.R.M., Torsvik, T.H., 2002. Earth geography from 500 to 400 million years ago: a faunal and palaeomagnetic review. J. Geol. Soc. Lond. 159, 631–644.
- Cooper, R.A., Sadler, P.M., Munnecke, A., Crampton, J.S., 2014. Graptoloid evolutionary rates track Ordovician-Silurian global climate change. Geol. Mag. 151, 349–364.
- Cramer, B.D., Saltzman, M.R., 2005. Sequestration of C-12 in the deep ocean during the early Wenlock (Silurian) positive carbon isotope excursion. Palaeogeogr. Palaeocl. 219, 333–349.
- Cramer, B.D., Saltzman, M.R., 2007. Fluctuations in epeiric sea carbonate production during Silurian positive carbon isotope excursions: a review of proposed paleoceanographic models. Palaeogeogr. Palaeocl. 245, 37–45.
- Cramer, B.D., Loydell, D.K., Samtleben, C., Munnecke, A., Kaljo, D., Mannik, P., Martma, T., Jeppsson, L., Kleffner, M.A., Barrick, J.E., Johnson, C.A., Emsbo, P., Joachimski, M.M., Bickert, T., Saltzman, M.R., 2010. Testing the limits of Paleozoic chronostratigraphic correlation via high-resolution (< 500 k.y.) integrated conodont, graptolite, and carbon isotope (delta C-13(carb)) biochemostratigraphy across the Llandovery-Wenlock (Silurian) boundary: is a unified Phanerozoic time scale achievable? Geol. Soc. Am. Bull. 122, 1700–1716.
- Crampton, J.S., Cooper, R.A., Sadler, P.M., Foote, M., 2016. Greenhouse-icehouse transition in the late Ordovician marks a step change in extinction regime in the marine plankton. P Natl. Acad. Sci. USA 113, 1498–1503.
- DeLange, G.J., Thomson, J., Reitz, A., Slomp, C.P., Principato, M.S., Erba, E., Corselli, C., 2008. Synchronous basin-wide formation and redox-controlled preservation of a Mediterranean sapropel. Nat. Geosci. 1, 606–610.
- Dickens, G.R., Owen, R.M., 1994. Late Miocene-early Pliocene Manganese Redirection in the Central Indian-Ocean expansion of the Intermediate Water Oxygen Minimum Zone. Paleoceanography 9, 169–181.
- Dickson, A., 2017. A molybdenum-isotope perspective on Phanerozoic deoxygenation events. Nat. Geosci. 10, 721–726.
- Edwards, C.T., Fike, D.A., Saltzman, M.R., Lu, W.Y., Lu, Z.L., 2018. Evidence for local and global redox conditions at an early Ordovician (Tremadocian) mass extinction. Earth Planet Sci. Lett. 481, 125–135.
- Fike, D.A., Bradley, A.S., Rose, C.V., 2015. Rethinking the ancient sulfur cycle. Ann. Rev. Earth Pl Sc. 43, 593–622.
- Finnegan, S., Bergmann, K., Eiler, J.M., Jones, D.S., Fike, D.A., Eisenman, I., Hughes, N.C., Tripati, A.K., Fischer, W.W., 2011. The Magnitude and Duration of late Ordovician-

- early Silurian Glaciation. Science 331, 903-906.
- Finnegan, S., Heim, N.A., Peters, S.E., Fischer, W.W., 2012. Climate change and the selective signature of the late Ordovician mass extinction. P Natl. Acad. Sci. USA 109, 6829–6834.
- Force, E.R., Cannon, W.F., 1988. Depositional Model for Shallow-Marine Manganese Deposits around Black Shale Basins. Econ. Geol. 83, 93–117.
- Force, E.R., Maynard, J.B., 1990. Manganese: Syngenetic deposits on the margins of anoxic basins. Rev. Econ. Geol. 5, 147–160.
- Frakes, L.A., Francis, J.E., Syktus, J.I., 1992. Climate Modes of the Phanerozoic. Cambridge University Press, Cambridge.
- Fryda, J., Storch, P., 2014. Carbon isotope chemostratigraphy of the Llandovery in northern peri-Gondwana: new data from the Barrandian area, Czech Republic. Est. J. Earth Sci. 63, 220–226.
- Ghienne, J.F., Desrochers, A., Vandenbroucke, T.R.A., Achab, A., Asselin, E., Dabard, M.P., Farley, C., Loi, A., Paris, F., Wickson, S., Veizer, J., 2014. A Cenozoic-style scenario for the end-Ordovician glaciation. Nat. Commun. 5.
- Gill, B.C., Lyons, T.W., Jenkyns, H.C., 2011a. A global perturbation to the sulfur cycle during the Toarcian Oceanic Anoxic Event. Earth Planet Sci. Lett. 312, 484–496.
- Gill, B.C., Lyons, T.W., Young, S.A., Kump, L.R., Knoll, A.H., Saltzman, M.R., 2011b. Geochemical evidence for widespread euxinia in the later Cambrian Ocean. Nature 469, 80–83.
- Gomes, M.L., Hurtgen, M.T., 2015. Sulfur isotope fractionation in modern euxinic systems: Implications for paleoenvironmental reconstructions of paired sulfate-sulfide isotope records. Geochim Cosmochim Ac 157, 39–55.
- Hammarlund, E.U., Dahl, T.W., Harper, D.A.T., Bond, D.P.G., Nielsen, A.T., Bjerrum, C.J., Schovsbo, N.H., Schonlaub, H.P., Zalasiewicz, J.A., Canfield, D.E., 2012. A sulfidic driver for the end-Ordovician mass extinction. Earth Planet Sci. Lett. 331, 128–139.
- Haq, B.U., Schutter, S.R., 2008. A chronology of Paleozoic Sea-level changes. Science 322, 64–68.
- Hardisty, D.S., Lyons, T.W., Riedinger, N., Isson, T.T., Owens, J.D., Aller, R.C., Rye, D.M., Planavsky, N.J., Reinhard, C.T., Gill, B.C., Masterson, A.L., Asael, D., Johnston, D.T., 2018. An Evaluation of Sedimentary Molybdenum and Iron as Proxies for Pore Fluid Paleoredox Conditions. Am. J. Sci. 318, 527–556.
- Harper, D.A.T., Hammarlund, E.U., Rasmussen, C.M.O., 2014. End Ordovician extinctions: a coincidence of causes. Gondwana Res. 25, 1294–1307.
- Hayes, J.M., Strauss, H., Kaufman, A.J., 1999. The abundance of C-13 in marine organic matter and isotopic fractionation in the global biogeochemical cycle of carbon during the past 800 Ma. Chem. Geol. 161, 103–125.
- Helbert, G.J., Lane, P.D., Owens, R.M., Siveter, D.J., Thomas, A.T., 1982. Lower Silurian trilobites from Norway. In: Worsley, D. (Ed.), IUGS Subcommission on Silurian Stratigraphy. Field Meeting, Oslo Region 1982. Paleontological Contributions from the University of Oslo, Oslo, pp. 129–146.
- Hints, O., Antonovits, L., Bauert, G., Nestor, V., Nolvak, J., Tammekand, M., 2018. CHITDB: a database for documenting and analysing diversification of Ordovician-Silurian chitinozoans in the Baltic region. Lethaia 51, 218–227.
- Jeppsson, L., 1997. The anatomy of the Mid–early Silurian Ireviken event and a scenario for P-S events. In: Brett, C.E., Baird, G.C. (Eds.), Paleontological Events: Stratigraphic, Ecological and Evolutionary Implications, pp. 451–492.
- Jeppsson, L., 1998. Silurian oceanic events: Summary of general characteristics. In: Landing, E., Johnson, M.E. (Eds.), Silurian Cycles: Linkages of Dynamic Stratigraphy with Atmospheric, Oceanic and Tectonic Changes. New York State Museum Bulletin, pp. 239–257.
- Joachimski, M.M., Pancost, R.D., Freeman, K.H., Ostertag-Henning, C., Buggisch, W., 2002. Carbon isotope geochemistry of the Frasnian-Famennian transition. Palaeogeogr. Palaeocl. 181, 91–109.
- Johnson, M.E., 2010. Tracking Silurian eustasy: alignment of empirical evidence or pursuit of deductive reasoning? Palaeogeogr. Palaeocl. 296, 276–284.
- Jones, D.S., Fike, D.A., 2013. Dynamic sulfur and carbon cycling through the end-Ordovician extinction revealed by paired sulfate-pyrite delta S-34. Earth Planet Sci. Lett. 363, 144–155.
- Jones, D.S., Martini, A.M., Fike, D.A., Kaiho, K., 2017. A volcanic trigger for the late Ordovician mass extinction? Mercury data from South China and Laurentia. Geology 45, 631–634.
- Kaljo, D., Martma, T., 2000. Carbon isotopic composition of Llandovery rocks (East Baltic Silurian) with environmental interpretation. Proceedings of the Estonian Academy of Sciences. Geology 49, 267–283.
- Kaljo, D., Martma, T., Mannik, P., Viira, V., 2003. Implications of Gondwana glaciations in the Baltic late Ordovician and Silurian and a carbon isotopic test of environmental cyclicity. B Soc. Geol. Fr 174, 59–66.
- Kienast, M., Calvert, S.E., Pelejero, C., Grimalt, J.O., 2001. A critical review of marine sedimentary delta C-13(org)-pCO(2) estimates: New palaeorecords from the South China Sea and a revisit of other low-latitude delta C-13(org)-pCO(2) records. Global Biogeochem. Cy 15, 113–127.
- Kiipli, E., 2004. Redox changes in the deep shelf of the East Baltic Basin in the Aeronian and early Telychian (early Silurian). Proceedings of the Estonian Academy of Sciences. Geology 53, 94–124.
- Kiipli, E., Kiipli, T., 2020. Hirnantian Sea-level changes in the Baltoscandian Basin, a review. Palaeogeogr. Palaeocl. 540, 1–13.
- Kiipli, E., Kiipli, T., Kallaste, T., 2004. Bioproductivity rise in the East Baltic epicontinental sea in the Aeronian (early Silurian). Palaeogeogr. Palaeocl. 205, 255–272.
- Kiipli, E., Kiipli, T., Kallaste, T., 2009. Reconstruction of currents in the Mid-Ordovicianearly Silurian Central Baltic Basin using geochemical and mineralogical indicators. Geology 37, 271–274.
- Kiipli, T., Kiipli, E., Kaljo, D., 2010. Silurian sea level variations estimated using SiO2/ Al2O3 and K2O/Al2O3 ratios in the Priekule drill core section, Latvia. Boll. Soc. Paleontol. Ital. 49, 55–63.

- Kiipli, T., Kallaste, T., Kiipli, E., Radzevicius, S., 2013. Correlation of Silurian bentonites based on the immobile elements in the East Baltic and Scandinavia. Gff 135, 152, 161.
- Kiipli, T., Radzevicius, S., Kallaste, T., 2014. Silurian bentonites in Lithuania: correlations based on sanidine phenocryst composition and graptolite biozonation - interpretation of volcanic source regions. Est. J. Earth Sci. 63, 18–29.
- Koren, T., Ahlberg, P., Nielsen, A.T., 2003. The post-persculptus and pre-ascensus graptolite fauna in Scania, South-Western Sweden: Ordovician or Silurian? INSUGEO, Serie Correlacion Geologica 18, 133–138.
- Kump, L.R., Arthur, M.A., Patzkowsky, M.E., Gibbs, M.T., Pinkus, D.S., Sheehan, P.M., 1999. A weathering hypothesis for glaciation at high atmospheric pCO₂ during the late Ordovician. Palaeogeogr. Palaeoclimatol. 152, 173–187.
- LaPorte, D.F., Holmden, C., Patterson, W.P., Loxton, J.D., Melchin, M.J., Mitchell, C.E., Finney, S.C., Sheets, H.D., 2009. Local and global perspectives on carbon and nitrogen cycling during the Hirnantian glaciation. Palaeogeogr. Palaeocl. 276, 182-105
- Lees, D.C., Fortey, R.A., Cocks, L.R.M., 2002. Quantifying paleogeography using biogeography: a test case for the Ordovician and Silurian of Avalonia based on brachiopods and trilobites. Paleobiology 28, 343–363.
- Loydell, D.K., 1994. Early Telychian changes in Graptoloid Diversity and Sea-Level. Geol. J. 29, 355–368.
- Loydell, D.K., 2007. Graptolites from the upper ordovician and lower silurian of Jordan. Sp Palaeont 5–66.
- Loydell, D.K., Mannik, P., Nestor, V., 2003. Integrated biostratigraphy of the lower Silurian of the Aizpute-41 core, Latvia. Geol. Mag. 140, 205–229.
- Lu, X.Z., Kendall, B., Stein, H.J., Li, C., Hannah, J.L., Gordon, G.W., Ebbestad, J.O.R., 2017. Marine redox conditions during deposition of late Ordovician and early Silurian organic-rich mudrocks in the Siljan ring district, Central Sweden. Chem. Geol. 457, 75–94.
- Lyons, T.W., 1997. Sulfur isotopic trends and pathways of iron sulfide formation in upper Holocene sediments of the anoxic Black Sea. Geochim Cosmochim Ac 61, 3367–3382.
- Lyons, T.W., Severmann, S., 2006. A critical look at iron paleoredox proxies: new insights from modern euxinic marine basins. Geochim Cosmochim Ac 70, 5698–5722.
- Lyons, T.W., Anbar, A.D., Severmann, S., Scott, C., Gill, B.C., 2009. Tracking euxinia in the ancient ocean: a multiproxy perspective and proterozoic case study. Annu. Rev. Earth Planet. Sci. 37, 507–534.
- Maletz, J., Ahlberg, P., Suyarkova, A., Loydell, D.K., 2014. Silurian graptolite biostratigraphy of the Rostanga-1 drill core, Scania - a standard for southern Scandinavia. Gff 136, 175–178.
- März, C., Poulton, S.W., Beckmann, B., Kuster, K., Wagner, T., Kasten, S., 2008. Redox sensitivity of P cycling during marine black shale formation: dynamics of sulfidic and anoxic, non-sulfidic bottom waters. Geochim Cosmochim Ac 72, 3703–3717.
- McAdams, N.E.B., Bancroft, A.M., Cramer, B.D., Witzke, B.J., 2017. Integrated carbon isotope and conodont biochemo-stratigraphy of the Silurian (Aeronian-Telychian) of the East-Central Iowa Basin, Iowa, USA. Newsl. Stratigr. 50, 391–416.
- Melchin, M.J., Holmden, C., 2006. Carbon isotope chemostratigraphy of the Llandovery in Arctic Canada: Implications for global correlation and sea-level change. Gff 128, 173–180.
- Melchin, M.J., Koren, T.N., Storch, P., 1998. Global diversity and survivorshippatterns of Silurian graptoloids. In: Landing, E., Johnson, M.E. (Eds.), Silurian Cycles: Linkages of Dynamic Stratigraphy with Atmospheric, Oceanic and Tectonic Changes, New York State Museum Bulletin. 491. pp. 165–181.
- Melchin, M.J., Mitchell, C.E., Holmden, C., Storch, P., 2013. Environmental changes in the late Ordovicianearly Silurian: Review and new insights from black shales and nitrogen isotopes. Geol. Soc. Am. Bull. 125, 1635–1670.
- Meyers, P.A, 1994. Preservation of elemental and isotopic source identification of sedimentary organic matter. Chem. Geol. 114, 289–302. https://doi.org/10.1016/0009-2541(94)90059-0.
- Miller, C.A., Peucker-Ehrenbrink, B., Walker, B.D., Marcantonio, F., 2011. Re-assessing the surface cycling of molybdenum and rhenium. Geochim Cosmochim Ac 75, 7146–7179.
- Munnecke, A., Mannik, P., 2009. New biostratigraphic and chemostratigraphic data from the Chicotte Formation (Llandovery, Anticosti Island, Laurentia) compared with the Viki core. Est. J. Earth Sci. 58, 159–169.
- Munnecke, A., Samtleben, C., Bickert, T., 2003. The ireviken event in the lower Silurian of Gotland, Sweden relation to similar palaeozoic and proterozoic events. Palaeogeogr. Palaeocl. 195, 99–124.
- Nehring-Lefeld, M., Modliński, Z., Swadowska, E., 1997. Thermal evolution of the Ordovician in the western margin of the East-European Platform: CAl and Ro data. Geol. Quar. 41, 129–138.
- Ostrander, C.M., Owens, J.D., Nielsen, S.G., 2017. Constraining the rate of oceanic deoxygenation leading up to a cretaceous Oceanic Anoxic Event (OAE-2: similar to 94 Ma). Sci. Adv. 3.
- Owens, J.D., Lyons, T.W., Li, X.N., Macleod, K.G., Gordon, G., Kuypers, M.M.M., Anbar, A., Kuhnt, W., Severmann, S., 2012. Iron isotope and trace metal records of iron cycling in the proto-North Atlantic during the Cenomanian-Turonian oceanic anoxic event (OAE-2). Paleoceanography 27.
- Owens, J.D., Gill, B.C., Jenkyns, H.C., Bates, S.M., Severmann, S., Kuypers, M.M.M., Woodfine, R.G., Lyons, T.W., 2013. Sulfur isotopes track the global extent and dynamics of euxinia during cretaceous Oceanic Anoxic Event 2. P Natl. Acad. Sci. USA 110, 18407–18412.
- Owens, J.D., Reinhard, C.T., Rohrssen, M., Love, G.D., Lyons, T.W., 2016. Empirical links between trace metal cycling and marine microbial ecology during a large perturbation to Earth's carbon cycle. Earth Planet Sci. Lett. 449, 407–417.
- Owens, J.D., Lyons, T.W., Hardisty, D.S., Lowery, C.M., Lu, Z., Lee, B., Jenkyns, H.C., 2017. Patterns of local and global redox variability during the Cenomanian–Turonian

- Boundary Event (Oceanic Anoxic Event 2) recorded in carbonates and shales from Central Italy. Sedimentology 64, 168–185.
- Pasquier, V., Sansjofre, P., Rabineau, M., Revillon, S., Houghton, J., Fike, D.A., 2017.
 Pyrite Sulfur Isotopes Reveal Glacial interglacial Environmental changes. P Natl.
 Acad. Sci. USA 114, 5941–5945.
- Patzkowsky, M.E., Slupik, L.M., Arthur, M.A., Pancost, R.D., Freeman, K.H., 1997. Late Middle Ordovician environmental change and extinction: Harbinger of the late Ordovician or continuation of Cambrian patterns? Geology 25, 911–914.
- Poulton, S.W., Canfield, D.E., 2005. Development of a sequential extraction procedure for iron: implications for iron partitioning in continentally derived particulates. Chem. Geol. 214, 209–221.
- Poulton, S.W., Canfield, D.E., 2011. Ferruginous Conditions: a Dominant Feature of the Ocean through Earth's history. Elements 7, 107–112.
- Poulton, S.W., Krom, M.D., Raiswell, R., 2004. A revised scheme for the reactivity of iron (oxyhydr)oxide minerals towards dissolved sulfide. Geochim Cosmochim Ac 68, 3703–3715.
- Present, T.M., Paris, G., Burke, A., Fischer, W.W., Adkins, J.F., 2015. Large Carbonate Associated Sulfate Isotopic Variability between Brachiopods, Micrite, and Other Sedimentary Components in late Ordovician Strata. Earth Planet Sci. Lett. 432, 187–198
- Raiswell, R., Canfield, D.E., 1996. Rates of reaction between silicate iron and dissolved sulfide in Peru margin sediments. Geochim Cosmochim Ac 60, 2777–2787.
- Raiswell, R., Newton, R., Bottrell, S.H., Coburn, P.M., Briggs, D.E.G., Bond, D.P.G., Poulton, S.W., 2008. Turbidite depositional influences on the diagenesis of Beecher's Trilobite Bed and the Hunsruck Slate; Sites of soft tissue pyritization. Am. J. Sci. 308, 105–129.
- Raiswell, R., Hardisty, D.S., Lyons, T.W., Canfield, D.E., Owens, J.D., Planavsky, N.J., Poulton, S.W., Reinhard, C.T., 2018. The Iron Paleoredox Proxies: a Guide to the pitfalls, Problems and proper Practice. Am. J. Sci. 318, 491–526.
- Rasmussen, C.M.O., Ullmann, C.V., Jakobsen, K.G., Lindskog, A., Hansen, J., Hansen, T., Eriksson, M.E., Dronov, A., Frei, R., Korte, C., Nielsen, A.T., Harper, D.A.T., 2016. Onset of main Phanerozoic marine radiation sparked by emerging Mid Ordovician icehouse. Sci. Rep. Uk 6.
- Rasmussen, C.M.O., Kroger, B., Nielsen, M.L., Colmenar, J., 2019. Cascading trend of early Paleozoic marine radiations paused by late Ordovician extinctions. P Natl. Acad. Sci. USA 116, 7207–7213.
- Reinhard, C.T., Planavsky, N.J., Robbins, L.J., Partin, C.A., Gill, B.C., Lalonde, S.V., Bekker, A., Konhauser, K.O., Lyons, T.W., 2013. Proterozoic Ocean redox and biogeochemical stasis. P. Natl. Acad. Sci. USA 110, 5357–5362.
- Richardson, J.A., Keating, C., Lepland, A., Hints, O., Bradley, A.S., Fike, D.A., 2019. Silurian records of carbon and sulfur cycling from Estonia: the importance of depositional environment on isotopic trends. Earth Planet Sci. Lett. 512, 71–82.
- Rose, C.V., Fischer, W.W., Finnegan, S., Fike, D.A., 2019. Records of carbon and sulfur cycling during the Silurian Ireviken event in Gotland, Sweden. Geochim Cosmochim Ac 246, 299–316.
- Royer, D.L., Berner, R.A., Beerling, D.J., 2001. Phanerozoic atmospheric CO2 change: evaluating geochemical and paleobiological approaches. Earth-Sci. Rev. 54, 349–392.
- Rue, E.L., Smith, G.J., Cutter, G.A., Bruland, K.W., 1997. The response of trace element redox couples to suboxic conditions in the water column. Deep-Sea Res Pt I 44, 113–134.
- Sahoo, S.K., Planavsky, N.J., Kendall, B., Wang, X.Q., Shi, X.Y., Scott, C., Anbar, A.D., Lyons, T.W., Jiang, G.Q., 2012. Ocean oxygenation in the wake of the Marinoan glaciation. Nature 489, 546–549.
- Sahoo, S.K., Planavsky, N.J., Jiang, G., Kendall, B., Owens, J.D., Wang, X., Shi, X., Anbar, A.D., Lyons, T.W., 2016. Oceanic oxygenation events in the anoxic Ediacaran Ocean. Geobiology 14, 457–468.
- Saltzman, M.R., Thomas, E., 2012. Carbon isotope stratigraphy. In: Geologic Time Scale 2012. vol 1 & 2. pp. 207–232.
- Scott, C., Lyons, T.W., 2012. Contrasting molybdenum cycling and isotopic properties in euxinic versus non-euxinic sediments and sedimentary rocks: refining the

- paleoproxies. Chem. Geol. 324, 19-27.
- Scott, C., Lyons, T.W., Bekker, A., Shen, Y., Poulton, S.W., Chu, X., Anbar, A.D., 2008. Tracing the stepwise oxygenation of the Proterozoic Ocean. Nature 452, 456–459.
- Sepkoski, J.J., Bambach, R.K., Raup, D.M., Valentine, J.W., 1981. Phanerozoic marine diversity and the fossil record. Nature 293 (5832), 435–437.
- Sheehan, P.M., 2001. The late Ordovician mass extinction. Annu. Rev. Earth Planet. Sci. 29, 331–364.
- Storch, P., 1995. Biotic crises and post-crisis recoveries recorded by Silurian planktonic graptolite faunas of the Barrandian area (Czech Republic). Geolines 3, 59–70.
- Them, T.R., Gill, B.C., Caruthers, A.H., Gerhardt, A.M., Grocke, D.R., Lyons, T.W., Marroquin, S.M., Nielsen, S.G., Alexandre, J.P.T., Owens, J.D., 2018. Thallium isotopes reveal protracted anoxia during the Toarcian (early Jurassic) associated with volcanism, carbon burial, and mass extinction. P Natl. Acad. Sci. USA 115, 6501.
- Thomsen, E., Baarli, B.G., 1982. Brachiopods of the lower Llandovery Saelabonn and Solvik formations of the Ringerike, Asker and Oslo districts. In: Worsley, D. (Ed.), lUGS Subcommission on Silurian Stratigraphy. Field Meeting, Oslo Region 1982. Paleontological Contributions from the University of Oslo, Oslo, pp. 63–77.
- Tribovillard, N., Algeo, T.J., Lyons, T., Riboulleau, A., 2006. Trace metals as paleoredox and paleoproductivity proxies: an update. Chem. Geol. 232, 12–32.
- Trotter, J.A., Williams, I.S., Barnes, C.R., Lecuyer, C., Nicoll, R.S., 2008. Did cooling oceans trigger Ordovician biodiversification? Evidence from conodont thermometry. Science 321, 550–554.
- Turgeon, S., Brumsack, H.J., 2006. Anoxic vs dysoxic events reflected in sediment geochemistry during the Cenomanian-Turonian Boundary Event (cretaceous) in the Umbria-Marche Basin of Central Italy. Chem. Geol. 234, 321–339.
- van Staal, C.R., Whalen, J.B., Valverde-Vaquero, P., Zagorevski, A.R.N., 2009. Pre-Carboniferous, episodic accretion-related, orogenesis along the Laurentian margin of the Northern Appalachians. In: Murphy, J.B., Keppie, J.B., Hynes, A.J. (Eds.), Ancient Orogens and Modern Analogues. Geological Society of London Special Publications, pp. 271–316.
- Vaquer-Sunyer, R., Duarte, C.M., 2010. Sulfide exposure accelerates hypoxia-driven mortality. Limnol. Oceanogr. 55, 1075–1082.
- Vecoli, M., Samuelsson, J., 2001. Quantitative evaluation of microplankton palaeobio-geography in the Ordovician-early Silurian of the northern Trans European Suture Zone: implications for the timing of the Avalonia-Baltica collision. Rev. Palaeobot. Palynol. 115, 43–68.
- Waid, C.B.T., Gramer, B.D., 2017. Global chronostratigraphic correlation of the Llandovery Series (Silurian System) in Iowa, USA, using high-resolution carbon isotope (delta(13) C-carb) chemostratigraphy and brachiopod and conodont biostratigraphy. B Geosci. 92, 373–390.
- Walasek, N., Loydell, D.K., Fryda, J., Mannik, P., Loveridge, R.F., 2018. Integrated graptolite-conodont biostratigraphy and organic carbon chemostratigraphy of the Llandovery of Kallholn quarry, Dalarna, Sweden. Palaeogeogr. Palaeocl. 508, 1–16.
- Wang, G., Zhan, R., Percival, I.G., 2019. The end-Ordovician mass extinction: A single-pulse event? Earth Sci. Rev. 192, 15–33. https://doi.org/10.1016/j.earscirev.2019. 01.023.
- Yan, D.T., Chen, D.Z., Wang, Q.C., Wang, J.G., 2012. Predominance of stratified anoxic Yangtze Sea interrupted by short-term oxygenation during the Ordo-Silurian transition. Chem. Geol. 291, 69–78.
- Young, S.A., Kleinberg, A., Owens, J.D., 2019. Geochemical evidence for expansion of marine euxinia during an early Silurian (Liandovery-Wenlock boundary) mass extinction. Earth Planet Sci. Lett. 513. 187–196.
- Zhang, T.G., Shen, Y.N., Zhan, R.B., Shen, S.Z., Chen, X., 2009. Large perturbations of the carbon and sulfur cycle associated with the late Ordovician mass extinction in South China. Geology 37, 299–302.
- Zou, C.N., Qiu, Z., Poulton, S.W., Dong, D.Z., Wang, H.Y., Chen, D.Z., Lu, B., Shi, Z.S., Tao, H.F., 2018. Ocean euxinia and climate change "double whammy" drove the late Ordovician mass extinction. Geology 46, 535–538.